

การวิเคราะห์วัสดุไร้ขอบเขตสามมิติโดยวิธีการคู่ควบระหว่างวิธีการไฟไนต์เอลิเมนต์และวิธีบาวน์
ดาร์เอลิเมนต์แบบเอกฐานอย่างอ่อน



นาย ศักดิ์ระวี ศรีภิรมย์

ศูนย์วิทยทรัพยากร
วิทยานิพนธ์นี้เป็นส่วนหนึ่งของการศึกษาตามหลักสูตรปริญญาวิศวกรรมศาสตรมหาบัณฑิต

สาขาวิชาวิศวกรรมโยธา ภาควิชาวิศวกรรมโยธา

คณะวิศวกรรมศาสตร์ จุฬาลงกรณ์มหาวิทยาลัย

ปีการศึกษา 2552

ลิขสิทธิ์ของจุฬาลงกรณ์มหาวิทยาลัย

A COUPLING OF FEM AND WEAKLY SINGULAR SGBEM FOR ANALYSIS OF A THREE-
DIMENSIONAL INFINITE MEDIUM



SAKRAVEE SRIPROM

A Thesis Submitted in Partial Fulfillment of the Requirements
for the Degree of Master of Engineering Program in Civil Engineering

Department of Civil Engineering

Faculty of Engineering

Chulalongkorn University

Academic Year 2009

Copyright of Chulalongkorn University

ศักดิ์ระวี ศรีภิรมย์: การวิเคราะห์วัตถุไร้ขอบเขตสามมิติโดยวิธีการคู่ควบระหว่างวิธีการไฟไนต์เอลิเมนต์และวิธีบาวด์ารีเอลิเมนต์แบบเอกฐานอย่างอ่อน. (A COUPLING OF FEM AND WEAKLY SINGULAR SGBEM FOR ANALYSIS OF A THREE-DIMENSIONAL INFINITE MEDIUM) อ.ที่ปรึกษาวิทยานิพนธ์หลัก: ผศ.ดร. จรุง รุ่งอมรรัตน์, 48 หน้า.

วิทยานิพนธ์ฉบับนี้เสนอระเบียบวิธีการคำนวณเชิงตัวเลขที่มีประสิทธิภาพ สำหรับการวิเคราะห์ปัญหาตัวกลางไร้ขอบเขตแบบสามมิติ โดยตัวกลางดังกล่าวอาจประกอบด้วย ปัญหาที่เป็นภาวะเอกฐาน อันเป็นผลจากรอยแตกและ/หรือบริเวณเฉพาะที่มีพฤติกรรมไร้เชิงเส้นอันเป็นผลเนื่องมาจากแรงกระทำที่ทำให้เกิดความเค้นสูง โดยทั่วไประเบียบวิธีบาวด์ารีเอลิเมนต์ไม่เหมาะสมที่จะนำมาวิเคราะห์ปัญหาตัวกลางที่มีบริเวณไร้เชิงเส้นอยู่ด้วย โดยในส่วนของวิเคราะห์ปัญหาตัวกลางไร้ขอบเขตหรือตัวกลางที่มีพื้นผิวไม่ต่อเนื่อง จำเป็นต้องอาศัยระเบียบวิธีการคำนวณเชิงตัวเลขแบบพิเศษ การศึกษานี้ได้พัฒนากระบวนการวิเคราะห์ปัญหาโดยใช้ระเบียบวิธีบาวด์ารีเอลิเมนต์แบบสมมาตรของการ์เลอจิน ควบคู่กับระเบียบวิธีไฟไนต์เอลิเมนต์แบบมาตรฐาน สำหรับขั้นตอนแรกของการวิเคราะห์ปัญหา ตัวกลางไร้ขอบเขตจะถูกแบ่งออกเป็น 2 โดเมนย่อย ได้แก่ โดเมนของไฟไนต์เอลิเมนต์ ซึ่งเป็นโดเมนที่มีขอบเขตจำกัดและครอบคลุมบริเวณเฉพาะที่มีพฤติกรรมไร้เชิงเส้น และโดเมนของบาวด์ารีเอลิเมนต์ซึ่งเป็นบริเวณไร้ขอบเขตและครอบคลุมบริเวณที่มีความไม่ต่อเนื่องของพื้นผิว การใช้ระเบียบวิธีบาวด์ารีเอลิเมนต์ในการวิเคราะห์บริเวณไร้ขอบเขตมีข้อดีเหนือกว่าระเบียบวิธีไฟไนต์เอลิเมนต์ เนื่องจากมีสมการควบคุมและมีกระบวนการแบ่งขอบเขตย่อยง่ายกว่า รวมทั้งสามารถใช้ประโยชน์จากคู่ของการกระจัดและหน่วยแรงในรูปแบบปริพันธ์มีความเป็นเอกฐานอย่างอ่อน ซึ่งมีลำดับเป็น $O(1/r)$ ทำให้เขตของฟังก์ชันพื้นฐานที่ใช้ในการประมาณค่าต้องต้องการความต่อเนื่องเป็นแบบ C^0 เท่านั้น การศึกษานี้ได้ทำการทดสอบความถูกต้องของระเบียบวิธีเชิงตัวเลขที่พัฒนา โดยทำการเปรียบเทียบกับงานวิจัยในอดีต นอกจากนี้ยังได้เสนอและวิจารณ์ผลการวิเคราะห์ปัญหาเชิงตัวเลขสำหรับกรณีปัญหาต่างๆ ด้วย

ภาควิชา วิศวกรรมโยธา

สาขาวิชา วิศวกรรมโยธา

ปีการศึกษา 2552

ลายมือชื่อนิสิต

ลายมือชื่อ อ.ที่ปรึกษาวิทยานิพนธ์หลัก

#4970596121 : MAJOR CIVIL ENGINEERING


KEYWORDS : INFINITE MEDIUM / CRACKS/ SGBEM/ FEM

SAKRAVEE SRIPROM: A COUPLING OF FEM AND WEAKLY SINGULAR
SGBEM FOR ANALYSIS OF A THREE-DIMENSIONAL INFINITE MEDIUM.

THESIS ADVISOR: ASSIST.PROF. JAROON RUNGAMORN RAT, Ph.D., 48 pp.

This thesis offers an efficient numerical technique for analysis of a three-dimensional infinite medium that contain both a line of singularity introduced by cracks and a localized nonlinear region introduced by high intensity loads. It is well-known that nonlinearities present within the domain render the modeling by methods of boundary integral equations computationally inefficient while treatment of a medium that is unbounded and/or contains the discontinuity surface requires special numerical treatments and can lead to a substantial computational cost. In this investigation, we establish a coupling procedure by exploiting advantageous features of both a standard finite element method (FEM) and a symmetric Galerkin boundary element method (SGBEM). The infinite medium is first decomposed into two sub-domains; the first one that is finite, localized, and may contain a nonlinear region is modeled by the FEM while the other that is unbounded and may contain the discontinuity surface is treated by the SGBEM. Use of boundary integral equations to treat an infinite region instead of the FEM offers two advantages; one corresponding to the mathematical ease of the governing equations and the numerical discretization effort (i.e. a set of governing equations involving only integrals over the boundary of the domain). Another key feature of the current technique is the use of a pair of weak-form integral equations for the displacement and for the traction to establish the formulation for the SGBEM. Such a pair of integral equations are weakly singular in the sense that they contain only kernels of order $O(1/r)$ and, as a consequence, they only require continuous interpolations in the approximation procedure. To demonstrate accuracy and versatility of the current technique, numerous numerical experiments are performed and numerical solutions for selected cases are reported and discussed.

Department : ..CIVIL ENGINEERING.....

Student's Signature 

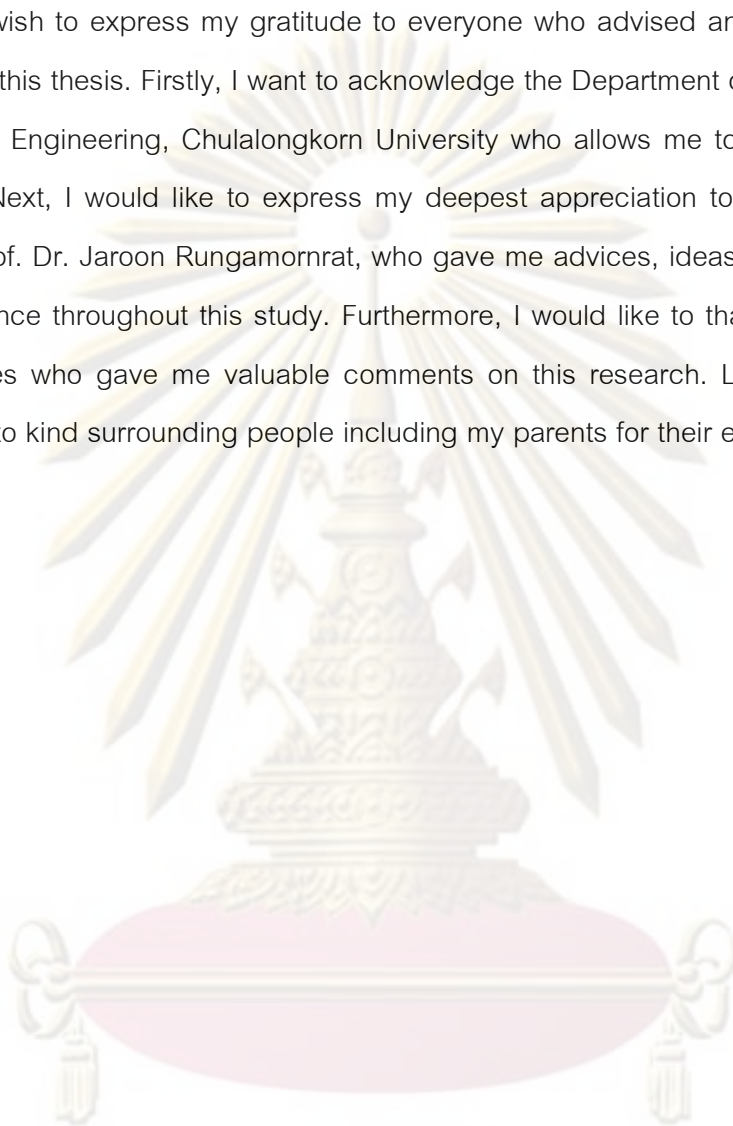
Field of Study : ..CIVIL ENGINEERING.....

Advisor's Signature 

Academic Year : ..2009.....

ACKNOWLEDGEMENTS

I wish to express my gratitude to everyone who advised and supported me to complete this thesis. Firstly, I want to acknowledge the Department of Civil Engineering, Faculty of Engineering, Chulalongkorn University who allows me to study for Master's Degree. Next, I would like to express my deepest appreciation to my thesis adviser, Assist. Prof. Dr. Jaron Rungamornrat, who gave me advices, ideas, intimate supports, and patience throughout this study. Furthermore, I would like to thank all of my thesis committees who gave me valuable comments on this research. Lastly, I feel deeply indebted to kind surrounding people including my parents for their endless support and love.

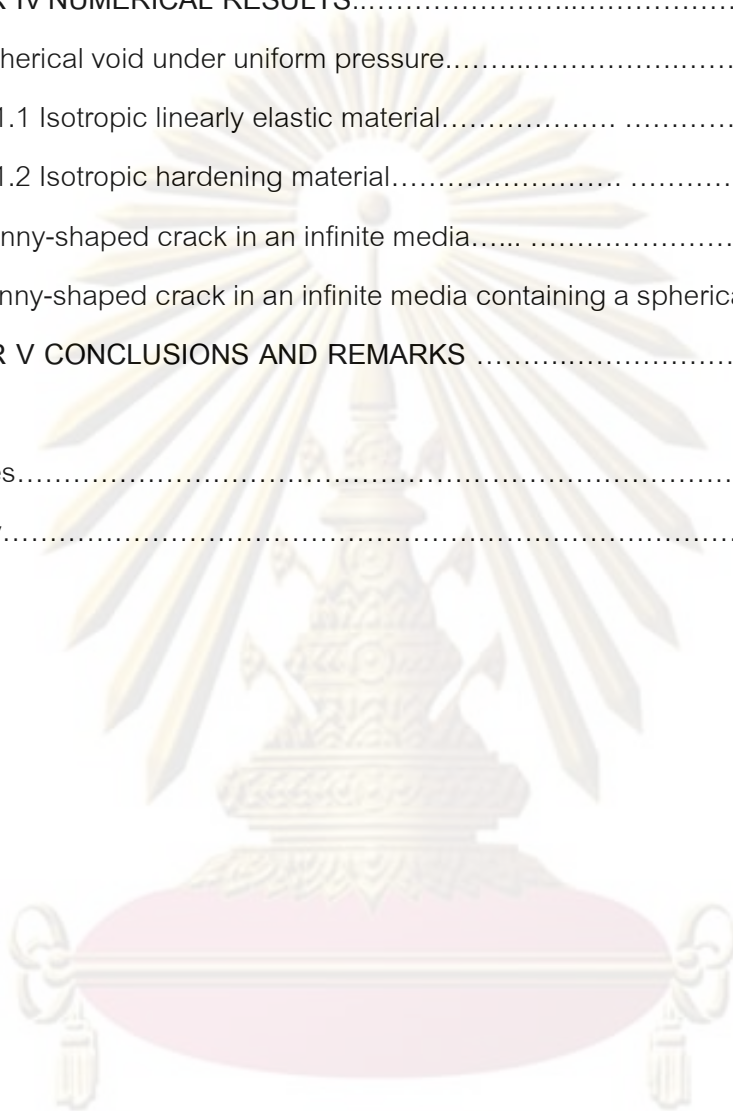


ศูนย์วิทยทรัพยากร
จุฬาลงกรณ์มหาวิทยาลัย

CONTENTS

	Page
Abstract (Thai).....	iv
Abstract (English).....	v
Acknowledgements.....	vi
Contents.....	vii
List of Tables.....	ix
List of Figures.....	x
List of Abbreviations.....	xiv
CHAPTER I INTRODUCTION.....	1
1.1 General.....	1
1.2 Background and Review.....	2
1.3 Research Objective.....	6
1.4 Research Scopes.....	6
1.5 Research Methodology.....	6
1.6 Research Significance	7
CHAPTER II PROBLEM FORMULATION.....	8
2.1 Governing equations for Ω^B	9
2.2 Governing equations for Ω^F	13
2.3 Symmetric governing equations for Ω	15
CHAPTER III NUMERICAL TREATMENTS	16
3.1 Discretization	16
3.1.1 Treatment of interface	18
3.2 Numerical integration	18
3.2.1 Regular double surface integral.....	18
3.2.2 Weakly singular double surface integral.....	19
3.2.3 Nearly singular double surface integral.....	19
3.3 Evaluation of weakly singular kernels.....	19
3.4 Linear and nonlinear solvers.....	20

	Page
3.5 Determination of stress intensity factors.....	21
3.6 Coupling of SGBEM with commercial FE package.....	23
CHAPTER IV NUMERICAL RESULTS.....	24
4.1 Spherical void under uniform pressure.....	25
4.1.1 Isotropic linearly elastic material.....	27
4.1.2 Isotropic hardening material.....	31
4.2 Penny-shaped crack in an infinite media.....	32
4.3 Penny-shaped crack in an infinite media containing a spherical void.....	36
CHAPTER V CONCLUSIONS AND REMARKS	43
References.....	45
Biography.....	48



ศูนย์วิทยทรัพยากร
 จุฬาลงกรณ์มหาวิทยาลัย

LIST OF TABLES

Table		Page
Table 4.1	Elastic constants of zinc and graphite-reinforced composite	34
Table 4.2	Normalized mode-I stress intensity factor for penny-shaped crack subjected to uniform normal traction	35



ศูนย์วิทยทรัพยากร
จุฬาลงกรณ์มหาวิทยาลัย

LIST OF FIGURES

	Page
Figure 2.1 Schematic of a three-dimensional infinite medium containing a crack and a localized nonlinear zone indicated by a shaded region	1
Figure 2.2 Schematic of an imaginary surface S_I used in the domain decomposition.....	9
Figure 2.3 Schematic of (a) the BEM-region Ω^B containing a crack and (b) the FEM-region containing a nonlinear zone Ω^F	9
Figure 3.1 Schematic of elements employed in the discretization of the BEM-region: (a) 9-node crack-tip elements, (b) 8-node quadratic elements, and (c) 6-node quadratic elements.....	17
Figure 3.2 Schematic of elements employed in the discretization of the FEM-region, (a) 20-node brick elements, and (b) 15-node prism elements.....	17
Figure 3.3 Local coordinate system for calculation of stress intensity factors..	22
Figure 4.1 Schematic of a three-dimensional infinite medium containing a spherical void of radius a	25
Figure 4.2 Relation between uniaxial stress and plastic strain of an isotropic hardening material.....	26
Figure 4.3 Decomposition of domain into BEM-region and FEM-region by a fictitious spherical surface of radius $5a$	26
Figure 4.4 Schematic of three meshes used in the analysis.....	27
Figure 4.5 Normalized radial displacement versus the normalized radial coordinate for isotropic, linearly elastic material with $\nu = 0.3$	28
Figure 4.6 Normalized radial stress versus the normalized radial coordinate for isotropic, linearly elastic material with $\nu = 0.3$	29

	Page
Figure 4.7	Normalized radial displacement versus the normalized radial coordinate for isotropic, linearly elastic material with $\nu = 0.3$. Results are obtained from Mesh 3 for both the coupling technique and the FE technique with domain truncation..... 30
Figure 4.8	Normalized radial stress versus the normalized radial coordinate for isotropic, linearly elastic material with $\nu = 0.3$. Results are obtained from Mesh 3 for both the coupling technique and the FE technique with domain truncation..... 30
Figure 4.9	Normalized radial displacement versus the normalized radial coordinate for isotropic hardening material with $E_2 = 0$ 32
Figure 4.10	Normalized radial stress versus the normalized radial coordinate for isotropic hardening material with $E_2 = 0$ 33
Figure 4.11	(a) Schematic of an infinite medium containing a penny-shaped crack, (b) crack under uniform normal traction σ_0 and (c) crack under uniform shear traction τ_0 33
Figure 4.12	Schematic of a selected FEM-region and the remaining BEM-region..... 34
Figure 4.13	Schematic of three meshes used in the analysis..... 35
Figure 4.14	Normalized mode-II and mode-III stress intensity factor for penny-shaped crack subjected to shear traction. Results are reported for isotropic material with $\nu = 0.3$ 36
Figure 4.15	mode-II and mode-III stress intensity factor for penny-shaped crack subjected to shear traction. Results are reported for zinc..... 37
Figure 4.16	mode-II and mode-III stress intensity factor for penny-shaped crack subjected to shear traction. Results are reported for graphite reinforced-composite..... 37
Figure 4.17	Schematic of a three-dimensional infinite medium containing a spherical void of radius a and a crack of radius a and subjected to uniform pressure at the surface of the void..... 38

	Page
Figure 4.18 Decomposition of domain into BEM-region and FEM-region by a fictitious spherical surface of radius $4a$	39
Figure 4.19 Schematic of three meshes used in the analysis.....	39
Figure 4.20 Normalized mode-I stress intensity factors for crack subjected to uniform pressure at the surface of void.....	40
Figure 4.21 Normalized mode-I stress intensity factor for crack subjected to uniform pressure at the surface of void. Results are reported for isotropic hardening material ($E_1 = E, E_2 = E/3$) with different levels of applied pressure.....	41
Figure 4.22 Maximum normalized mode-I stress intensity factor versus the level of applied pressure at the surface of void. Results are reported for an isotropic linearly elastic and two isotropic hardening materials.....	42



ศูนย์วิทยทรัพยากร
 จุฬาลงกรณ์มหาวิทยาลัย

CHAPTER 1

INTRODUCTION

1.1 General

A physical modeling of a three-dimensional solid by employing a mathematical domain that occupies the full space is standard and has extensively been used when responses of interest are localized in a zone with its length scale much smaller than that of the body. Influence of the outer boundary of such the domain is generally insignificant and can be discarded in the modeling without loss of accuracy. Such situations arise in various engineering applications, e.g. prediction of crack growth in hydraulic fracturing process where the fracture is generally treated as an isolated crack in an infinite medium, evaluation and assessment of service lifespan of large scale structures under cyclic loading where influence of initial defect of the structures can be characterized by prescribed small flaws, investigation of effective properties of materials possessing a microstructure (e.g. cracks, voids, inclusions), etc. One attractive aspect of using an infinite space as a representative domain is its mathematical ease associated with ignoring the remote boundary and this, as a consequence, allows certain boundary value problems admit analytical or close form solutions. For (most) problems where analytical solutions cannot readily be obtained, such an idealization significantly reduces complexity of the mathematical model in terms of both theoretical and numerical treatments in comparison with that involving a finite domain.

Although an infinite domain is employed in the idealization, complexity of the mathematical model still exists if the body contains a line of singularity. This situation arises when a surface of displacement discontinuities such as cracks and dislocations is contained in the body. Within the context of linear elasticity, the induced stress field in the vicinity of the crack front is relatively complicate and, in fact, the stresses are singular along such crack front. An extensive stress analysis of this cracked body to extract essential fracture information along the crack boundary generally requires

special theoretical and numerical treatments, especially when the problem is formulated within the context of a three-dimensional boundary value problem. Another source of complexity is due to the presence of localized, complex zones within the domain. These complex zones may arise naturally in various situations, for instance, a plastic zone induced by the application of high intensity loads in a small region, containment of small defects and inhomogeneities, influence of nonmechanical effects on localized regions, etc. The stress and displacement fields in those zones and their immediate surrounding regions can obviously be complex and essentially need careful considerations.

Beside the necessity to integrate such complexity described above into the mathematical model in order to capture the physical phenomena of interest to a level of sufficient accuracy, it poses, at the same time, theoretical and computational challenges to treat such complex boundary value problems. A focus of this current investigation is on the development of a mathematical and numerical model to accurately capture the behavior of an infinite body containing both cracks and localized complex zones.

1.2 Background and review

An analytical approach has extensively been used for analysis of stress in a solid body; however, its application is still restricted to situations where the body can be treated either within the context of a two-dimensional boundary value problem or within the context of a relatively simple three-dimensional problem (e.g. Timoshenko and Goodier, 1951; Fabrikant, 1989; Fabrikant, 1991). This limitation becomes more apparent when the level of complexity of the physical phenomena of interest increases (e.g. presence of nonlinearities, inhomogeneities, singularities, etc.). A physically-sound and sophisticated mathematical model must be employed in order to capture such complex behavior and, due to this complexity, the analytical or exact solution to this boundary value problem cannot readily be constructed. As a consequence, it necessitates the use of numerical techniques developed specifically to serve this purpose.

The finite element method (FEM) and the boundary element method (BEM) are two, robust numerical techniques mostly used in the modeling of various field problems. Both techniques possess a wide range of applications and there are situations that favor FEM over BEM and vice versa. The FEM has proven to be an efficient and powerful method for modeling a broad class of problems in structural and solid mechanics (e.g. Oden and Carey, 1984; Hughes, 2000; Zienkiewicz and Taylor, 2000). The formulation of the FEM is sufficiently general allowing nonlinearities and non-homogeneities present in the domain be treated. In addition, a final system of equations resulting from this method possesses a desirable form (e.g. symmetry, sparseness, and positive definiteness of the coefficient matrix). Nevertheless, the FEM contains major drawbacks and requires nontrivial treatments when applied to certain classes of problems. For instance, if the problem involves an infinite domain, use of a standard discretization procedure to such domain is impractical. To remove this difficulty, a domain may be truncated into a region that has finite dimensions; however, it still remains to define the suitable truncated surface and to impose appropriate boundary conditions on that surface. Another drawback results from that, when the standard FEM is directly applied to model crack problems, it has a limited capability to obtain adequately accurate fracture information (viz. stress intensity factors) with use of reasonably coarse meshes. This weakness becomes more apparent when mixed-mode problems are concerned. In general, it requires a substantially fine mesh in a region surrounding the crack front to achieve stress intensity factors of sufficient accuracy (e.g. Swenson and Ingraffea, 1988; Martha *et al.*, 1993; Ayhan *et al.*, 2003).

Boundary element method (BEM) is efficient and attractive for modeling certain classes of problems since, for a domain that is free of distributed sources or body force, the governing equation involves only integrals on the boundary of the domain (e.g. Cruse, 1988; Bonnet, 1995; Xu and Ortiz, 1993; Li *et al.*, 1998; Xu, 2000; Rungamornrat, 2006; Rungamornrat and Mear, 2008). As a consequence, the discretization effort is significantly reduced due to the reduction of dimensions of the problem by one. One advantage of the method over the FEM is its capability to model an infinite domain. In this situation, the remote boundary can be discarded without loss

via an appropriate treatment of remote conditions (e.g. Xu and Ortiz, 1993; Xu, 2000; Rungamornrat, 2006; Rungamornrat and Mear, 2008). A particular methodology which has proven highly successful for analysis of three-dimensional, uncracked bodies (e.g. Bonnet, 1995; Xiao, 1998), analysis of isolated cracks in three-dimensional, isotropic and anisotropic, linearly elastic infinite media (e.g. Xu and Ortiz, 1993; Li *et al.*, 1998; Xu, 2000; Rungamornrat, 2006; Rungamornrat and Mear, 2008), and analysis of cracks in three-dimensional, isotropic and anisotropic, linearly elastic finite bodies (e.g. Li *et al.*, 1998; Frangi *et al.*, 2002; Rungamornrat, 2006; Rungamornrat and Mear, 2008) is a weakly-singular, symmetric Galerkin boundary element method (SGBEM). The superior features of this technique over other types of the BEM are that all kernels appearing in the governing integral equations are only weakly singular of $\mathcal{O}(1/r)$ and that a system of linear algebraic equations resulting from discretization has a symmetric coefficient matrix. Since the involved kernels are weakly-singular of $\mathcal{O}(1/r)$, validity of the integral equations requires only that the boundary displacement data is continuous, hence allowing standard C^0 interpolations be employed in the numerical approximation. It has been demonstrated, in addition, that the weakly-singular SGBEM along with the proper treatment of singular field near the crack front yields highly accurate fracture information (viz. stress intensity factors) even relatively coarse meshes are employed in the discretization (e.g. Li *et al.*, 1998; Rungamornrat, 2006; Rungamornrat and Mear, 2008). While the weakly singular SGBEM yields very accurate numerical solutions for analysis of elasticity and fracture problems, it still contains unfavorable features and has limited capability of solving certain classes of problems. For instance, the method becomes inefficient or practically impossible for modeling problems involving nonlinearity or inhomogeneity. As the geometry of the domain becomes increasingly complex and the size of the problem becomes large (e.g. a large number of elements is required to discretize the entire boundary of the domain), the method tends to become computationally expensive (in terms of both computational time and storage) in comparison with the standard Galerkin finite element method (FEM). Although the SGBEM gives rise to a symmetric coefficient matrix, the matrix itself is dense and each of its entries must be computed by means of a double surface integration. Another crucial drawback of the boundary integral equation techniques is due to the lack of

generality of the key formulation to treat nonlinearities and inhomogeneities in an efficient manner.

In the past two decades, several attempts have been put into the development of an efficient numerical procedure that exploits advantages of both the BEM and the FEM for modeling two-dimensional and three-dimensional elasticity and fracture problems. The idea is to decompose the domain into two parts; the first part that is localized, possesses linear behavior, and may contain a surface of discontinuities (e.g. cracks and dislocations) is modeled by the boundary element methods, and the second part that may be nonlinear and nonhomogeneous and occupy the majority of the domain is treated by the finite element methods. Within the context of linear elasticity, there has been various investigations directed toward coupling of the conventional BEM and the standard FEM (e.g. Schnack and Turke, 1997; Elleithy *et al.*, 2001; Elleithy and Tanaka, 2003) and toward coupling of the strongly singular SGBEM and the standard FEM (e.g. Ganguly *et al.*, 2000; Haas and Kuhn, 2003; Yu, 2003). Note that the former coupling gives rise to a system of linear equations with a nonsymmetric coefficient matrix while the latter requires special numerical considerations for treatment of strongly singular integrals (e.g. Gray *et al.*, 1990; Martin and Rizzo, 1996). An extensive review of various types of coupling between the boundary element methods and the finite element methods can be found in the work of Bonnet *et al.* (1998). A particular symmetric coupling strategy between the weakly-singular SGBEM and the FEM was first formulated by Xiao (1998) to treat cracks in isotropic, linearly elastic finite bodies. In his development, a pair of weakly singular, weak-form displacement and traction integral equations was utilized along with the principle of virtual work and the proper treatment of continuity conditions on the interface to establish the symmetric formulation. Later, Frangi and Novati (2003) successfully implemented Xiao's formulation to model cracked bodies subjected to pure traction boundary conditions. However, in their technique, the discretization of the interface between the two regions (one treated by the standard FEM and the other treated by the SGBEM) was still restricted to matching or conforming meshes. Rungamornrat (2004) generalized the work of Li *et al.* (1998) to incorporate the material anisotropy and treatment of non-matching interface. On the basis of an

extensive literature survey, a coupling between the weakly singular SGBEM and the standard FEM that is capable of modeling a whole space with embedded isolated cracks and localized zones of complex behavior is still not available and the current investigation is proposed with a primary objective to fill this gap of knowledge.

1.3 Research Objective

The proposed research aims primarily to develop an efficient and accurate numerical technique capable of modeling an infinite solid medium that may contain displacement discontinuities (e.g. cracks and dislocations) and a region possessing complex behavior (e.g. localized nonlinear zone). The developed computational tool is then employed to investigate various boundary value problems of interest such as fracture problems.

1.4 Scope of Research

The development is established within the context of three-dimensional infinite media. The domain is restricted only to one that can be decomposed into two separate regions: a localized, finite region that may exhibit complex behavior and a (complementary) region that is unbounded, linearly elastic, free of body force and remote loading and may contain isolated cracks.

1.5 Research Methodology

The domain decomposition technique is proposed to partition an infinite body into two separate regions: a localized complex region and a complementary unbounded region. The governing equation of the former region is obtained in terms of a weak-form equation using the well-known principle of virtual work while, for the latter region, the governing equations are developed based on a pair of weakly singular, weak-form displacement and traction integral equations. The governing equations for the entire domain are obtained by combining the two sets of equations through the proper use of continuity conditions on the interface.

For the numerical treatment, a standard Galerkin approximation is proposed to discretize the entire set of governing equations. In particular, discretization of the localized complex region follows a standard procedure of the finite element method (FEM) while discretization of the complementary unbounded region exploits a well-known strategy called the weakly singular, symmetric Galerkin boundary element method (SGBEM). To enhance the modeling capability of the proposed technique, vast features of a reliable commercial finite element package is employed to treat the localized complex region.

1.6 Research Significance

The current investigation proposes a robust SGBEM-FEM coupling technique that is well-suited for treatment of a three-dimensional, infinite medium containing isolated cracks and localized complex regions. The attractive feature of the proposed technique is to utilize vast features of the FEM to treat the localized, complex regions and the weakly-singular, SGBEM to efficiently and accurately model an unbounded region containing a line of singularity (e.g. crack front). Use of weakly singular integral equations as a basis of the SGBEM formulation offers an ease in the numerical treatment, e.g. the choice of interpellants and numerical integration. An outcome of the study, the in-house computer program, offers an alternative, robust numerical tool capable of performing stress analysis of a three-dimensional infinite medium containing cracks and localized complex zones. The program is, in addition, supplemented by an efficient and accurate algorithm to extract the essential fracture information, e.g. the stress intensity factors.

Another benefit of the current investigation is that it offers insight into the SGBEM-FEM coupling strategy both in terms of the implementation procedure and its performance and this, therefore, constitutes a basis for the development of a coupling between the SGBEM and the commercial finite element software to further enhance the modeling capability.

CHAPTER 2

PROBLEM FORMULATION

Consider a three-dimensional, anisotropic, linearly elastic infinite body Ω containing a crack and a localized nonlinear zone as shown schematically in Figure 2.1. The two (geometrically coincident) surfaces of the crack are denoted by S_C^+ and S_C^- with their unit normal (taken to be directed 'into' the crack) satisfying $\mathbf{n}^+ = \mathbf{n}^-$, and, for convenience, we select $S_C \equiv S_C^+$ as a single surface to be utilized in representing the crack. Throughout the development carried out below, the body is assumed to be free of a body force and free of loading on its remote boundary, and both surfaces of the cracks are subjected to prescribed symmetric tractions $\mathbf{t}_C^+ = -\mathbf{t}_C^- \equiv \mathbf{t}_C$. In addition, the entire domain is assumed to be homogeneous, linearly elastic except in the localized region where nonlinearities and inhomogeneities can pertain.

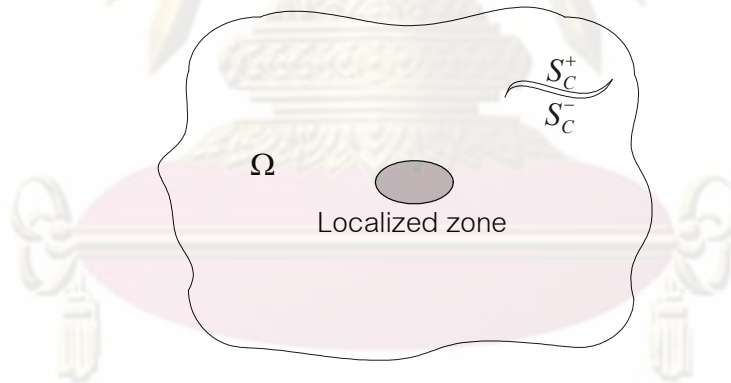


Figure 2.1 Schematic of a three-dimensional infinite medium containing a crack and a localized nonlinear zone indicated by a shaded region.

Now, let us partition the domain Ω along an imaginary surface S_I as indicated in Figure 2.2. This decomposition yields two sub-regions called a 'BEM-region' which is denoted by Ω^B and a 'FEM-region' which is denoted by Ω^F . The interface S_I is selected such that the FEM-region is finite and contains a localized complex zone while the BEM-region is unbounded and contains a crack as depicted in Figure 2.3. While the development presented further below is restricted only to a domain containing

a single crack and a single nonlinear zone, the formulation can readily be extended to treat multiple cracks and multiple nonlinear zones as long as the nonlinear zones are contained within one or more FEM-regions.

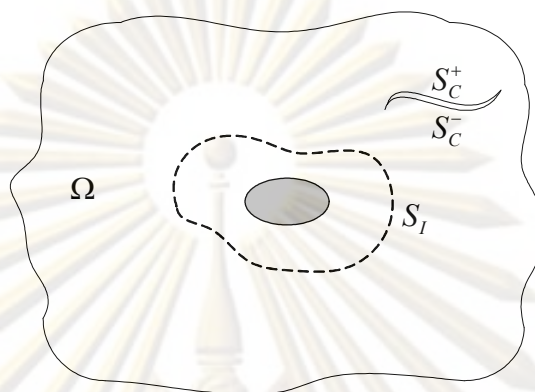


Figure 2.2 Schematic of an imaginary surface S_I used in the domain decomposition

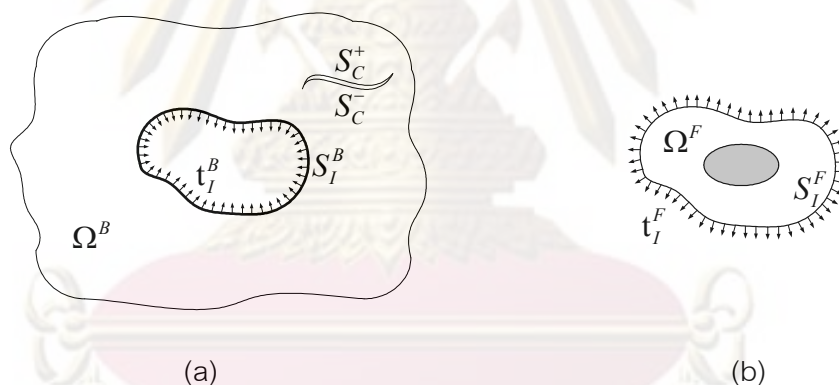


Figure 2.3 Schematic of (a) the BEM-region Ω^B containing a crack and (b) the FEM-region containing a nonlinear zone Ω^F

2.1 Governing equations for Ω^B

Consider first the BEM-region Ω^B . The total boundary of this region, denoted by S , consists of the crack surface S_C on which the traction is fully prescribed and the interface S_I where neither the traction nor the displacement is known a priori. To clearly demonstrate the role of the interface between the two sub-regions in the formulation given below, we denote \mathbf{t}_I^B and \mathbf{u}_I^B as the unknown traction and unknown displacement on the interface of Ω^B , respectively.

As a basis for the development of a set of governing integral equations for the BEM-region Ω^B , a pair of weakly singular, weak-form displacement and traction integral equations developed by Rungamornrat and Mear (2008) is employed. These two integral equations were derived from standard boundary integral relations for the displacement and stress along with a systematic regularization technique. The final form of the completely regularized integral equations is given in a form well-suited for establishing the symmetric formulation stated further below. Such pair of weak-form integral equations, when specialized to Ω^B , takes the form

$$\begin{aligned} \frac{1}{2} \int_{S_I} \tilde{t}_k(\mathbf{y}) u_k(\mathbf{y}) dS(\mathbf{y}) &= \int_{S_I} \tilde{t}_k(\mathbf{y}) \int_{S_I} U_i^k(\boldsymbol{\xi}-\mathbf{y}) t_i(\boldsymbol{\xi}) dS(\boldsymbol{\xi}) dS(\mathbf{y}) \\ &+ \int_{S_I} \tilde{t}_k(\mathbf{y}) \int_S G_{mj}^k(\boldsymbol{\xi}-\mathbf{y}) D_m v_j(\boldsymbol{\xi}) dS(\boldsymbol{\xi}) dS(\mathbf{y}) \\ &- \int_{S_I} \tilde{t}_k(\mathbf{y}) \int_S n_i(\boldsymbol{\xi}) H_{ij}^k(\boldsymbol{\xi}-\mathbf{y}) v_j(\boldsymbol{\xi}) dS(\boldsymbol{\xi}) dS(\mathbf{y}) \end{aligned} \quad (2.1)$$

$$\begin{aligned} - \int_S c(\mathbf{y}) \tilde{v}_k(\mathbf{y}) t_k(\mathbf{y}) dS(\mathbf{y}) &= \int_S D_i \tilde{v}_k(\mathbf{y}) \int_S C_{mj}^{ik}(\boldsymbol{\xi}-\mathbf{y}) D_m v_j(\boldsymbol{\xi}) dS(\boldsymbol{\xi}) dS(\mathbf{y}) \\ &+ \int_S D_i \tilde{v}_k(\mathbf{y}) \int_{S_I} G_{ik}^j(\boldsymbol{\xi}-\mathbf{y}) t_j(\boldsymbol{\xi}) dS(\boldsymbol{\xi}) dS(\mathbf{y}) \\ &- \int_S \tilde{v}_k(\mathbf{y}) \int_{S_I} n_l(\mathbf{y}) H_{lk}^j(\boldsymbol{\xi}-\mathbf{y}) t_j(\boldsymbol{\xi}) dS(\boldsymbol{\xi}) dS(\mathbf{y}) \end{aligned} \quad (2.2)$$

where \tilde{t}_k and \tilde{v}_k are sufficiently smooth test functions, $D_m(\cdot)$ is a surface differential operator defined by

$$D_m(\cdot) = n_i \varepsilon_{ism} \frac{\partial(\cdot)}{\partial \xi_s}, \quad (2.3)$$

$v_j(\boldsymbol{\xi})$ is defined by

$$v_j(\boldsymbol{\xi}) = \begin{cases} u_j(\boldsymbol{\xi}), & \boldsymbol{\xi} \in S_I \\ \Delta u_j(\boldsymbol{\xi}), & \boldsymbol{\xi} \in S_C \end{cases} \quad (2.4)$$

with $\Delta u_j(\boldsymbol{\xi}) = u_j^+(\boldsymbol{\xi}) - u_j^-(\boldsymbol{\xi})$ denoting the jump in the displacement across the discontinuity surface (i.e. the relative displacement of the two geometrically coincident surfaces associated with the displacement discontinuity), and the geometry-dependent constant $c(\mathbf{y})$ is defined by

$$c(\mathbf{y}) = \begin{cases} 1/2 & , \mathbf{y} \in S_I \\ 1 & , \mathbf{y} \in S_C \end{cases} \quad (2.5)$$

The kernel $H_{ij}^p(\boldsymbol{\xi} - \mathbf{y})$ is independent of material properties and is given explicitly by

$$H_{ij}^p(\boldsymbol{\xi} - \mathbf{y}) = -\frac{1}{4\pi} \frac{(\xi_i - y_i) \delta_{pj}}{r^3} \quad (2.6)$$

where δ_{pj} is a standard Kronecker-delta tensor, and the kernels $U_i^p(\boldsymbol{\xi} - \mathbf{y})$, $G_{mj}^p(\boldsymbol{\xi} - \mathbf{y})$ and $C_{mj}^{tk}(\boldsymbol{\xi} - \mathbf{y})$ are given, for generally anisotropic materials, by

$$U_i^p(\boldsymbol{\xi} - \mathbf{y}) = K_{mp}^{mi}(\boldsymbol{\xi} - \mathbf{y}) \quad (2.7)$$

$$G_{mj}^p(\boldsymbol{\xi} - \mathbf{y}) = \varepsilon_{abm} E_{ajdc} K_{cp}^{bd}(\boldsymbol{\xi} - \mathbf{y}) \quad (2.8)$$

$$C_{mj}^{tk}(\boldsymbol{\xi} - \mathbf{y}) = A_{mjdn}^{tkoe} K_{dn}^{oe}(\boldsymbol{\xi} - \mathbf{y}) \quad (2.9)$$

where E_{ijkl} are elastic moduli and A_{mjdn}^{tkoe} and $K_{jl}^{ik}(\boldsymbol{\xi} - \mathbf{y})$ are defined by

$$A_{mjdn}^{tkoe} = \varepsilon_{pam} \varepsilon_{pbt} \left(E_{bknd} E_{ajeo} - \frac{1}{3} E_{ajkb} E_{dneo} \right) \quad (2.10)$$

$$K_{jl}^{ik}(\boldsymbol{\xi} - \mathbf{y}) = \frac{1}{8\pi^2 r} \oint_{\mathbf{z} \cdot \mathbf{r} = 0} (\mathbf{z}, \mathbf{z})_{kl}^{-1} z_i z_j ds(\mathbf{z}) \quad (2.11)$$

in which $\mathbf{r} = \boldsymbol{\xi} - \mathbf{y}$, $r = \|\mathbf{r}\|$, $(\mathbf{z}, \mathbf{z})_{jk} = z_i E_{ijkl} z_i$ and the integral is to be evaluated over a unit circle $\|\mathbf{z}\| = 1$ on a plane normal to the position vector \mathbf{r} . It is evident from (2.6)-(2.9) that the kernels $n_i H_{ij}^p(\boldsymbol{\xi} - \mathbf{y})$, $U_i^p(\boldsymbol{\xi} - \mathbf{y})$, $G_{mj}^p(\boldsymbol{\xi} - \mathbf{y})$ and $C_{mj}^{tk}(\boldsymbol{\xi} - \mathbf{y})$ are weakly

singular of $\mathcal{O}(1/r)$ (see details in Xiao (1998) for discussion of the singularity nature of the kernel $H_{ij}^p(\xi - \mathbf{y})$).

For the special case of isotropy, the kernels $U_i^p(\xi - \mathbf{y})$, $G_{mj}^p(\xi - \mathbf{y})$ and $C_{mj}^{tk}(\xi - \mathbf{y})$ reduces to

$$U_i^p(\mathbf{r}) = \frac{1}{16\pi(1-\nu)\mu} \left[\frac{(3-4\nu)}{r} \delta_{pi} + \frac{r_p r_i}{r^3} \right] \quad (2.12)$$

$$G_{mj}^p(\mathbf{r}) = \frac{1}{8\pi(1-\nu)r} \left[(1-2\nu) \varepsilon_{mpj} + \varepsilon_{ijm} \frac{r_i r_p}{r^2} \right] \quad (2.13)$$

$$C_{mj}^{tk}(\mathbf{r}) = \frac{\mu}{4\pi(1-\nu)r} \left[(1-\nu) \delta_{tk} \delta_{mj} + 2\nu \delta_{km} \delta_{jt} - \delta_{kj} \delta_{tm} - \frac{r_j r_k}{r^2} \delta_{tm} \right] \quad (2.14)$$

where ν is Poisson's ratio, μ is the elastic shear modulus, and ε_{ijk} is a standard alternating symbol defined by

$$\varepsilon_{ijk} = \begin{cases} 1 & , \quad ijk = 123, 231, 312 \\ -1 & , \quad ijk = 213, 132, 321 \\ 0 & , \quad otherwise \end{cases} \quad (2.15)$$

Toward obtaining a symmetric system of governing integral equations for the BEM-region Ω^B , we apply the weak-form traction integral equation (2.2) to the crack surface S_C (with $\tilde{\mathbf{v}} = 0$ on S_I) and to the interface S_I (with $\tilde{\mathbf{v}} = 0$ on S_C) and apply the weak-form displacement integral equation (2.1) to the interface S_I . A final set of integral equations is given by

$$\begin{aligned} \mathcal{A}_{CC}(\tilde{\mathbf{v}}, \Delta \mathbf{u}) + \mathcal{B}_{IC}(\mathbf{t}_I^B, \tilde{\mathbf{v}}) + \mathcal{A}_{CI}(\tilde{\mathbf{v}}, \mathbf{u}_I^B) &= -2\mathcal{F}_C^B(\tilde{\mathbf{v}}, \mathbf{t}_c) \\ \mathcal{B}_{IC}(\tilde{\mathbf{t}}_I^B, \Delta \mathbf{u}) + \mathcal{C}_{II}(\tilde{\mathbf{t}}_I^B, \mathbf{t}_I^B) + \mathcal{D}_{II}(\tilde{\mathbf{t}}_I^B, \mathbf{u}_I^B) &= 0 \\ \mathcal{A}_{IC}(\tilde{\mathbf{u}}_I^B, \Delta \mathbf{u}) + \mathcal{D}_{II}(\mathbf{t}_I^B, \tilde{\mathbf{u}}_I^B) + \mathcal{A}_{II}(\tilde{\mathbf{u}}_I^B, \mathbf{u}_I^B) &= -2\mathcal{F}_I^B(\tilde{\mathbf{u}}_I^B, \mathbf{t}_I^B) \end{aligned} \quad (2.16)$$

in which $\{\tilde{\mathbf{u}}_I^B, \tilde{\mathbf{t}}_I^B\}$ are test functions defined on the interface S_I , and where (with subscripts $p, q \in \{I, c\}$ introduced to specify the surface of integration) the bilinear integral operators \mathcal{A}_{pQ} , \mathcal{B}_{IC} , \mathcal{C}_{II} , \mathcal{D}_{II} and \mathcal{F}_p^B are defined by

$$\mathcal{A}_{pQ}(\mathbf{X}, \mathbf{Y}) = \int_{S_p} D_I X_k(\mathbf{y}) \int_{S_Q} C_{mj}^{tk}(\xi - \mathbf{y}) D_m Y_j(\xi) dS(\xi) dS(\mathbf{y}) \quad (2.17)$$

$$\begin{aligned} \mathcal{B}_{IC}(\mathbf{X}, \mathbf{Y}) &= \int_{S_I} X_k(\mathbf{y}) \int_{S_C} G_{mj}^k(\xi - \mathbf{y}) D_m Y_j(\xi) dS(\xi) dS(\mathbf{y}) \\ &- \int_{S_I} X_k(\mathbf{y}) \int_{S_C} n_m(\xi) H_{mj}^k(\xi - \mathbf{y}) Y_j(\xi) dS(\xi) dS(\mathbf{y}) \end{aligned} \quad (2.18)$$

$$\mathcal{C}_{II}(\mathbf{X}, \mathbf{Y}) = \int_{S_I} X_I(\mathbf{y}) \int_{S_I} U_i^I(\xi - \mathbf{y}) Y_i(\xi) dS(\xi) dS(\mathbf{y}) \quad (2.19)$$

$$\mathcal{F}_p^B(\mathbf{X}, \mathbf{Y}) = \frac{1}{2} \int_{S_p} X_i(\mathbf{y}) Y_i(\mathbf{y}) dS(\mathbf{y}) \quad (2.20)$$

$$\mathcal{D}_{II}(\mathbf{X}, \mathbf{Y}) = \mathcal{B}_{II}(\mathbf{X}, \mathbf{Y}) - \mathcal{F}_I^B(\mathbf{X}, \mathbf{Y}) \quad (2.21)$$

Note that the linear operators $\mathcal{A}_{pQ}(\mathbf{X}, \mathbf{Y})$ are in a symmetric form satisfying

$$\mathcal{A}_{pQ}(\mathbf{X}, \mathbf{Y}) = \mathcal{A}_{Qp}(\mathbf{Y}, \mathbf{X}) \quad (2.22)$$

and, as a consequence, the left hand side of the system of equations (2.16) is in a symmetric form. The tractions on the interface are not prescribed and as such the quantity $2\mathcal{F}_I^B(\tilde{\mathbf{u}}_I^B, \tilde{\mathbf{t}}_I^B)$ which appears on the right hand side of (2.16) does not constitute a loading term; this term will be addressed after the formulation for Ω^F is presented.

2.2 Governing equations for Ω^F

We now consider the FEM-region Ω^F . Note that the entire boundary of this region is the interface S_I on which both the traction and the displacement are unknown a priori. Here, we denote the traction and the displacement on the interface S_I

by \mathbf{u}_I^F and \mathbf{t}_I^F , respectively, in order to distinguish them from the quantities on the interface of the BEM-region Ω^B . Continuity of the displacements and tractions across the interface leads to the relations between the two sets of quantities:

$$\mathbf{t}_I^F = -\mathbf{t}_I^B \quad (2.23)$$

$$\mathbf{u}_I^F = \mathbf{u}_I^B \quad (2.24)$$

The weak-form equation governing the FEM-region Ω^F can readily be obtained using the principle of virtual work and the resulting equation is given by

$$\mathcal{K}_{FF}(\tilde{\mathbf{u}}, \boldsymbol{\sigma}) = 2\mathcal{F}_I^F(\tilde{\mathbf{u}}_I^F, \mathbf{t}_I^F) \quad (2.25)$$

in which $\boldsymbol{\sigma}$ is a stress tensor, $\tilde{\mathbf{u}}$ is a suitably well-behaved test function, $\tilde{\mathbf{u}}_I^F$ is the restriction of $\tilde{\mathbf{u}}$ on S_I , and

$$\mathcal{K}_{FF}(\tilde{\mathbf{u}}, \boldsymbol{\sigma}) = \int_{\Omega^F} \sigma_{ij}(\mathbf{y}) \left[\frac{\partial \tilde{u}_i}{\partial y_j}(\mathbf{y}) \right] dV(\mathbf{y}) \quad (2.26)$$

$$\mathcal{F}_I^F(\tilde{\mathbf{u}}_I^F, \mathbf{t}_I^F) = \frac{1}{2} \int_{S_I} \tilde{u}_{li}^F(\mathbf{y}) t_{li}^F(\mathbf{y}) dS(\mathbf{y}) \quad (2.27)$$

It is noted that a form of the stress tensor depends primarily on the material constitutive employed. For in stance, if the FEM-region is made of linearly elastic material, the stress tensor can be expressed directly in terms of elastic constants E_{ijkl} and the displacement \mathbf{u} , and the integral operator (2.25) becomes

$$\mathcal{K}_{FF}(\tilde{\mathbf{u}}, \mathbf{u}) = \int_{\Omega^F} E_{ijkl} \left[\frac{\partial \tilde{u}_i}{\partial y_j}(\mathbf{y}) \right] \left[\frac{\partial u_k}{\partial y_l}(\mathbf{y}) \right] dV(\mathbf{y}) \quad (2.28)$$

We remark that the factor of one-half in (2.27) has been introduced for convenience to cast this term in a form analogous to that for $\mathcal{F}_p^B(\mathbf{X}, \mathbf{Y})$ given by (2.20), and this then

leads to the factor of two appearing on the right hand side of (2.25). It is also worth noting that the operator \mathcal{F}_I^F is defined on a portion of the boundary of Ω^F whereas \mathcal{F}_I^B is defined on a portion of the boundary of Ω^B ; this distinction will be particularly important in what follows.

2.3 Symmetric governing equations for Ω

A set of governing equations of the entire domain Ω can readily be obtained by combining the weak-form equation (2.25) and a set of weakly-singular, weak-form integral equations (2.16). In particular, the last equation of (2.16) is subtracted by equation (2.25) and this leads to

$$\begin{aligned} \mathcal{A}_{CC}(\tilde{\mathbf{v}}, \Delta \mathbf{u}) + \mathcal{B}_{IC}(\mathbf{t}_I^B, \tilde{\mathbf{v}}) + \mathcal{A}_{CI}(\tilde{\mathbf{v}}, \mathbf{u}_I^B) &= -2\mathcal{F}_C^B(\tilde{\mathbf{v}}, \mathbf{t}_c) \\ \mathcal{B}_{IC}(\tilde{\mathbf{t}}_I^B, \Delta \mathbf{u}) + \mathcal{C}_{II}(\tilde{\mathbf{t}}_I^B, \mathbf{t}_I^B) + \mathcal{D}_{II}(\tilde{\mathbf{t}}_I^B, \mathbf{u}_I^B) &= 0 \\ \mathcal{A}_{IC}(\tilde{\mathbf{u}}_I^B, \Delta \mathbf{u}) + \mathcal{D}_{II}(\mathbf{t}_I^B, \tilde{\mathbf{u}}_I^B) + [\mathcal{A}_{II} - \mathcal{K}_{FF}] &= \mathcal{E} \end{aligned} \quad (2.29)$$

in which

$$[\mathcal{A}_{II} - \mathcal{K}_{FF}] = \mathcal{A}_{II}(\tilde{\mathbf{u}}_I^B, \mathbf{u}_I^B) - \mathcal{K}_{FF}(\tilde{\mathbf{u}}, \boldsymbol{\sigma}) \quad (2.30)$$

and where \mathcal{E} is given by

$$\mathcal{E} = -2 \left[\mathcal{F}_I^B(\tilde{\mathbf{u}}_I^B, \mathbf{t}_I^B) + \mathcal{F}_I^F(\tilde{\mathbf{u}}_I^F, \mathbf{t}_I^F) \right] \quad (2.31)$$

Upon invoking strong continuity of both the traction and the displacement test functions across the interface, i.e. $\mathbf{t}_I^F = -\mathbf{t}_I^B$ and $\tilde{\mathbf{u}}_I^F = \tilde{\mathbf{u}}_I^B$, it can readily be verified that $\mathcal{E} = 0$. As a consequence, equation (2.25) is in a symmetric form provided that \mathcal{K}_{FF} is a symmetric integral operator. A set of equations (2.29) is employed as the key governing equations for the boundary value problem currently treated.

CHAPTER 3

NUMERICAL TREATMENTS

This chapter briefly summarizes numerical procedure employed to construct numerical solutions of the boundary value problem formulated in chapter 2. The discretization of the BEM-region, the FEM-region and the interface between the two regions is first discussed. Then, components essential for numerical evaluation of weakly singular and nearly singular double surface integrals and for determination of general mixed-mode stress intensity factors are presented. Finally, the key strategy for establishing the coupling between the in-house weakly singular SGBEM code and the reliable commercial finite element package is discussed.

3.1 Discretization

Standard Galerkin approximation is proposed to discretize the system of equations (2.29). For the BEM-region Ω^B , only the single crack surface S_C and the interface S_I require discretization. In the neighborhood of the crack front, special nine-node crack-tip elements enriched by proper shape functions are employed to accurately capture asymptotic fields near the singularity zone. This special type of elements was originated by Li *et al.* (1998) for analysis of cracks in isotropic, linearly elastic media and further generalized by Rungamornrat and Mear (2008) to take the material anisotropy into account. Use of these special elements renders relatively coarse meshes be used in the local zone near the crack with numerical results of sufficient accuracy. In addition to the high order approximation feature of the interpolation functions, extra degrees of freedom are introduced at the edge of the element to directly represent the gradient of the relative crack-face displacement. This then allows the mixed-mode stress intensity factors (i.e. mode-I, mode-II and mode-III stress intensity factors) be calculated directly in terms of those extra degrees of freedom. Extensive discussion can be found in the work of Li *et al.* (1998) and Rungamornrat and Mear (2008). For the current investigation, nine-node special crack tip elements (indicated in

Figure 3.1(a)) are employed to discretize the crack front. Both the majority of the crack surface (excluding the crack front) and the interface of the BEM-region are discretized by standard, isoparametric, eight-node or six-node C^0 elements as shown schematically in Figure. 3.1(b)-(c).

For the FEM-region Ω^F , standard three-dimensional, isoparametric C^0 elements (e.g. fifteen-node prism elements and twenty-node brick elements as shown schematically in Figure. 3.2) are used throughout in the domain discretization.

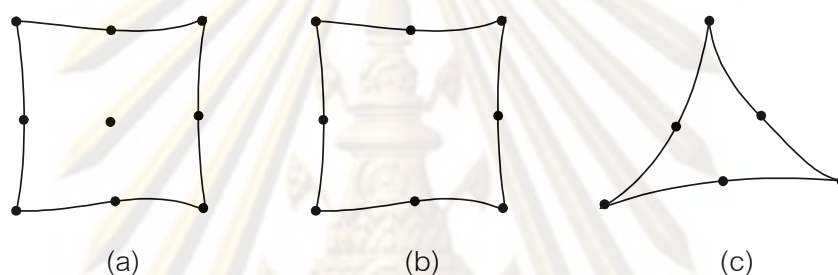


Figure 3.1 Schematic of elements employed in the discretization of the BEM-region: (a) 9-node crack-tip elements, (b) 8-node quadratic elements, and (c) 6-node quadratic elements

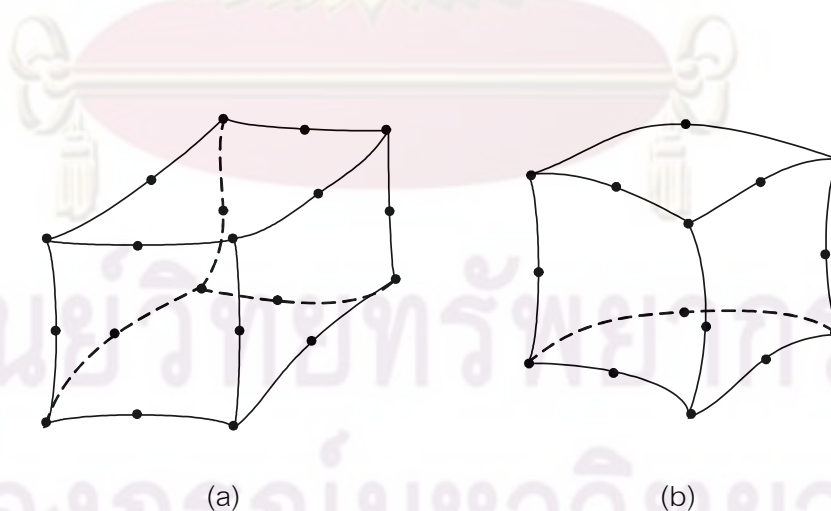


Figure 3.2 Schematic of elements employed in the discretization of the FEM-region, (a) 20-node brick elements, and (b) 15-node prism elements

3.1.1 Treatment of interface

The BEM-region and the FEM-region are discretized such that meshes on the interface of the two regions conform (i.e. the two discretized interfaces are geometrically identical). A simple means to generate these conforming meshes is to discretize the FEM-region first and then use its surface mesh as the interface mesh of the BEM-region. With this strategy, all nodal points on both discretized interfaces are coincident. The key advantage of using conforming meshes is that the strong continuity of the displacement, the traction, and the test functions across the interface can be enforced exactly and, as a result, the condition $\mathcal{E} = \mathbf{0}$ is also satisfied exactly in the discretization level.

For convenience in the assembly process, numbering of all nodes on the interface of the BEM-region and the interface of the FEM-region is chosen to be identical. This numbering scheme automatically generates the same degrees of freedom for any two nodes on both interfaces with the same coordinates; as a consequence, the continuity across the interface is enforced.

3.2 Numerical integration

For the FEM-region, all integrals arising from the discretization of the weak-form equation contain only regular integrands and, as a result, they can be efficiently and accurately integrated by standard Gaussian quadrature. In the contrary, numerical evaluation of integrals arising from the discretization of the BEM-region is nontrivial since it involves the treatment of three types of double surface integrals: regular integrals, weakly singular integrals and nearly singular integrals. The numerical integration for the first type is standard while the last two types require special care.

3.2.1 Regular double surface integral

The regular double surface integral arises when a pair of outer and inner elements resulting from the discretization is remote relative to the characteristic dimension of the two elements (i.e. the distance between any source and field points is

relatively large when compared with the size of the two elements). This therefore renders its integrand nonsingular and well-behaved, and such integral can accurately and efficiently be integrated by standard Gaussian quadrature.

3.2.2 Weakly singular double surface integral

The weakly singular double surface integral arises when the outer and inner elements resulting from the discretization are coincident. Its integrand is therefore singular and of order $1/r$. This particular type of integrals can be integrated efficiently by using special quadratures based on a triangular polar transformation (see details in the work of Hayami and Brebbia (1988) and Xiao (1998)). Such variable transformation is utilized primarily to supply the jacobian of transformation to remove the $1/r$ -singularity. To further regularize the integrand to reduce the possible rapid variation resulting from the triangular polar transformation, an additional variable transformation based on a logarithmic family suggested by Xiao (1998) is utilized. The final double surface integral contains only regular and well-behaved integrand proper for integrating by Gaussian quadrature.

3.2.3 Nearly singular double surface integral

The most challenging task is to evaluate nearly singular integrals that arise when the two surfaces of integration are relatively close but not coincident. The integrand exhibits rapid variation and this renders the numerical integration by a standard Gaussian quadrature inefficient (see Xiao, 1998). To improve the accuracy of the numerical integration, the triangular polar transformation is employed first and then followed by a series of logarithmic transformations in both radial and angular directions to regularize the rapid-variation integrand. The resulting integral is well-suited for being integrated by a standard Gaussian quadrature (e.g. Hayami and Brebbia, 1988; Xiao, 1998).

3.3 Evaluation of weakly singular kernels

In addition to the regularization procedure to eliminate the singularity and smoothen the rapid variation of integrands of double surface integrals, another important

aspect needs to be considered is the efficient evaluation of all involved kernels $\{n_m(\boldsymbol{\xi})H_{mj}^p(\boldsymbol{\xi}-\mathbf{y}), n_m(\mathbf{y})H_{mj}^p(\boldsymbol{\xi}-\mathbf{y}), U_i^p(\boldsymbol{\xi}-\mathbf{y}), G_{mj}^p(\boldsymbol{\xi}-\mathbf{y}), C_{mj}^{tk}(\boldsymbol{\xi}-\mathbf{y})\}$. For the first two kernels $n_m(\boldsymbol{\xi})H_{mj}^p(\boldsymbol{\xi}-\mathbf{y})$ and $n_m(\mathbf{y})H_{mj}^p(\boldsymbol{\xi}-\mathbf{y})$, they involve the computation of unit normal vector \mathbf{n} and an explicit and simple function H_{mj}^p . This can readily be achieved via a standard procedure. For the last three kernels, they admit explicit form in terms of ordinary functions for isotropic linear elastic materials (see equations (2.12)-(2.14)) and, as a consequence, their values can readily be obtained. In the contrary, the kernels $U_i^p(\boldsymbol{\xi}-\mathbf{y})$, $G_{mj}^p(\boldsymbol{\xi}-\mathbf{y})$ and $C_{mj}^{tk}(\boldsymbol{\xi}-\mathbf{y})$ for general anisotropy are expressed in terms of a line integral over a unit circle (see equations (2.7)-(2.9)). Direct evaluation of such the line integral for every pair of points $(\boldsymbol{\xi}, \mathbf{y})$ arising from the numerical integration is obviously computationally expensive. To avoid this massive computation, we adopt a well-known strategy, called the interpolation technique (e.g. Rungamornrat, 2006; Rungamornrat and Mear, 2008), to approximate values of those kernels. Specifically, the interpolant of each kernel is constructed based on a two-dimensional grid using standard quadratic shape functions. Values of kernels at all grid points are obtained by performing direct numerical integration of the line integral (2.11) via Gaussian quadrature and then using the relations (2.7)-(2.9). The accuracy of such approximation can readily be controlled by the refinement of the interpolation grid. Extensive discussion of this interpolation scheme can be found in the work of Rungamornrat (2004) and Rungamornrat and Mear (2008).

3.4 Linear and nonlinear solvers

For linear elastic boundary value problems, the discretization yields a system of linear algebraic equations. A coefficient matrix is essentially symmetric but non-definite (i.e. it contains both positive and negative eigenvalues). The latter feature results from that both the displacement and traction integral equations are employed along the interface. For an in-house coupling code implemented, a Jacobi-preconditioning conjugate gradient method is utilized to solve such system of linear equations. While coefficient matrix is non-definite, it has been found in various numerical experiments that the method yields a converged solution with relatively small number of iterations. For a coupling between the SGBEM and the commercial FE package, a

system of linear equations is solved directly by a linear solver provided by the FE package.

For nonlinear boundary value problems, only the coupling between the SGBEM and the commercial FE package is implemented (see details in section 3.6). A system of nonlinear algebraic equations resulting from the discretization is solved directly by a nonlinear solver of FE package.

3.5 Determination of stress intensity factors

For linear fracture analysis, the primary quantities of interest are stress intensity factors; this fracture data provides a measure of the dominant behavior of the stress field in the vicinity of the crack front and it is an essential ingredient for predicting fracture initiation, propagation pattern and fatigue assessment. With use of special crack-tip elements to approximate field quantities in the neighborhood of the crack front, it additionally provides an accurate means to extract the mix-mode stress intensity factors along the crack front. This feature results from the fact that the special crack-tip element contains extra degrees of freedom along the crack front and their values correspond directly to the gradient of the relative crack-face displacement. Once the system of linear or nonlinear equations is solved, nodal quantities along the crack front are extracted and then used to compute all stress intensity factors.

An explicit expression for the mixed-mode stress intensity factors in terms of data along the crack front, local geometry near the crack boundary and the material properties can be found in the work of Li *et al.* (1998) for cracks in isotropic materials and Rungamornrat and Mear (2008) for cracks in general anisotropic materials. In the current investigation, the formula proposed by Rungamornrat and Mear (2008) is implemented for both cracks embedded in isotropic and generally anisotropic media. Such explicit expression is briefly discussed below.

Consider a crack-tip element located along the crack front where \mathbf{x}_c denotes a node located on the crack front, $\{x_1, x_2, x_3\}$ is a local cartesian coordinate system centered at \mathbf{x}_c and $\{\mathbf{e}_1, \mathbf{e}_2, \mathbf{e}_3\}$ is a set of orthonormal base vectors as shown

schematically in Figure. 3.3. The mixed-mode stress intensity factors at the point \mathbf{x}_c is given by

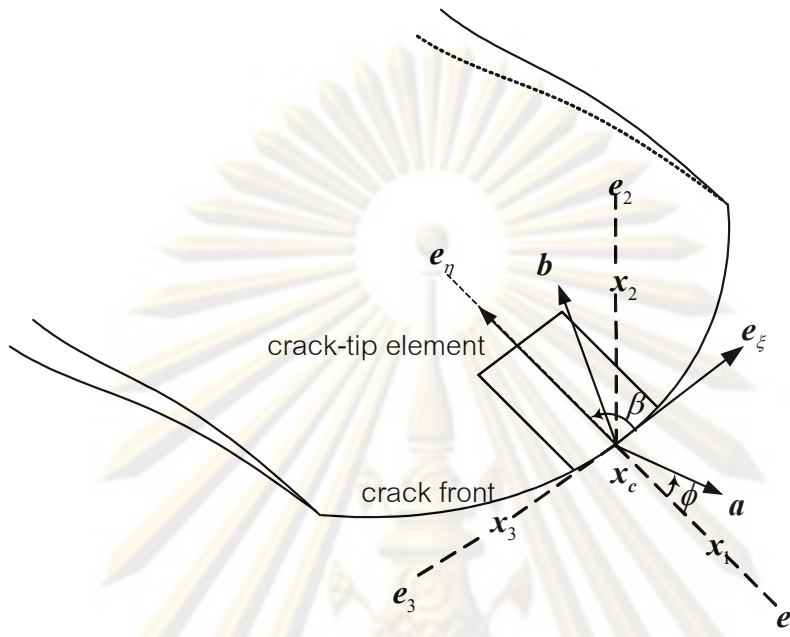


Figure 3.3 Local coordinate system for calculation of stress intensity factors

$$k_i(\mathbf{x}_c) = \sqrt{\frac{\pi}{2J \sin \beta}} B_{im}(\mathbf{x}_c) u_m^*(\mathbf{x}_c) \quad (3.1)$$

where $u_m^*(\mathbf{x}_c)$ is the quantity at the point \mathbf{x}_c defined in terms of extra degrees of freedom along the crack front by

$$u_m^*(\mathbf{x}_c) = \sum_i u_{m(i)}^e \psi_i(\xi_c, -1), \quad (3.2)$$

with the summation taken over all nodes of an element, $u_{m(i)}^e$ representing the components of nodal data at the i^{th} node, $(\xi_c, -1)$ denoting the natural coordinates of \mathbf{x}_c , and $\psi_i(\xi_c, -1)$ corresponding to the value of a standard element shape function associated with the i^{th} node evaluated at the point \mathbf{x}_c . An angle β and a constant J are defined by

$$\sin \beta = -\mathbf{e}_n \cdot \mathbf{e}_1, \quad (3.3)$$

$$\mathbf{e}_n = \frac{1}{J} \frac{\partial \mathbf{r}_c}{\partial \eta}(\xi_c, -1), \quad (3.4)$$

$$J = \left\| \frac{\partial \mathbf{r}_c}{\partial \eta}(\xi_c, -1) \right\|, \quad (3.5)$$

$$\mathbf{r}_c(\xi, n) = \mathbf{x}(\xi, n) - \mathbf{x}_c. \quad (3.6)$$

It is important to point out that the formula (3.1) allows the mixed-mode stress intensity factors be computed only in terms of data at nodes located on the crack front. This is due to the fact that $\psi_i(\xi_c, -1)$ vanishes for nodes not on the crack front. Details of derivation of the expression (3.1) are referred to the work of Li et al. (1998) and Rungamornrat and Mear (2008).

3.6 Coupling of SGBEM with commercial FE package

To enhance the modeling capability, the weakly singular SGBEM is then coupled with a reliable, commercial finite element code. The key objective is to exploit vast features of the FE package (e.g. mesh generation, user-defined elements, powerful linear and nonlinear solvers, and various material models, etc.) to treat a complex, localized FEM-region and utilize the SGBEM in-house code to supply information associated with the majority of the domain that is unbounded and possibly contains isolated discontinuities.

In the coupling process, the BEM-region is first discretized to obtain a system of linear algebraic equations. The corresponding coefficient matrix and the vector involving the prescribed data are constructed using the in-house code and they can be viewed as a stiffness matrix and a load vector of a 'super element' containing all degrees of freedom of the BEM-region. This piece of information is then imported into the FE package via a user-defined subroutine (UEL) and then assembled with element

stiffness matrices contributed from the discretized FEM-region. Since meshes of both interfaces (one associated with the BEM-region and the other corresponding to the FEM-region) are conforming, the assembly procedure can readily be achieved by using numbering strategy. Specifically, nodes on the interface of the BEM-region are named identical to nodes on the interface of the FEM-region (associated with the same displacement degrees of freedom). It is worth noting that each interface node of the BEM-region possesses six degrees of freedom (i.e. three displacement degrees of freedom and three traction degrees of freedom) but there are only three (displacement) degrees of freedom per interface node of the FEM-region. To overcome this difficulty, the interface node of the BEM-region is treated as a double node where the first node is chosen to represent the displacement degrees of freedom and is named the same as the interface node of the FEM-region while the second node is fictitiously chosen with different name to represent the traction degrees of freedom. By this means, the assembling procedure follows naturally that for a standard finite element.

Once the coupling analysis is complete, nodal quantities associated with the BEM-region are extracted from the output file generated by the FE package and then post-processed. For instance, the displacement and stress within the BEM-region can readily be computed from the standard displacement and stress boundary integral relations, and the stress intensity factors can be calculated from the explicit expression (3.1).

CHAPTER 4

NUMERICAL RESULTS

As a means to verify both the formulation and the numerical implementations, we first perform numerical experiments on boundary value problems in which the analytical solution exists. In the analysis, a series of mesh refinement is adopted in order to investigate both the convergence and accuracy of the numerical solutions. Once the method is verified, it is then applied to solve more complex boundary value problems that may not have a close form solution in order to demonstrate its capability and versatility. For brevity of the presentation, a selected set of results are reported and discussed.

4.1 Spherical void under uniform pressure

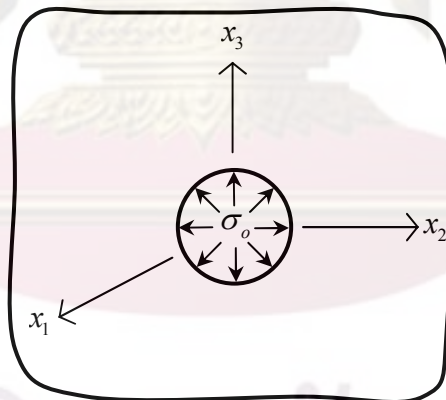


Figure 4.1 Schematic of a three-dimensional infinite medium containing a spherical void of radius a

Consider a spherical void of radius a embedded in a three-dimensional infinite medium as shown schematically in Figure 4.1. The void is subjected to the uniform normal traction (i.e. uniform pressure) σ_0 . In the numerical experiments, two material models are investigated: one associated with an isotropic, linearly elastic

material with Young's modulus E and Poisson ratio $\nu = 0.3$ and the other corresponding to an isotropic hardening material with the uniaxial stress-strain relation shown in Figure 4.2. E_1 and E_2 denote the modulus of the elastic zone and the modulus of the hardening part, respectively, and σ_y denotes the initial yielding stress.

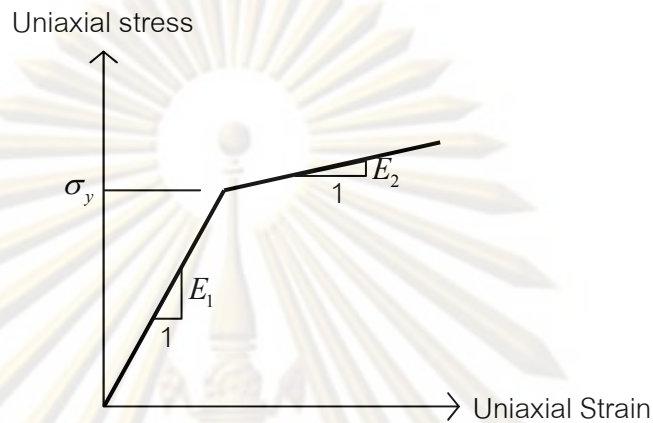


Figure 4.2 Relation between uniaxial stress and plastic strain of an isotropic hardening material

To test the coupling technique, we first decompose the body into two regions by a fictitious spherical surface of radius $5a$ and centered at the origin as shown by a dashed line in Figure 4.3. It is important to remark that such a surface must be chosen relatively large to ensure that the inelastic zone that may exist is fully contained in the FEM-region.

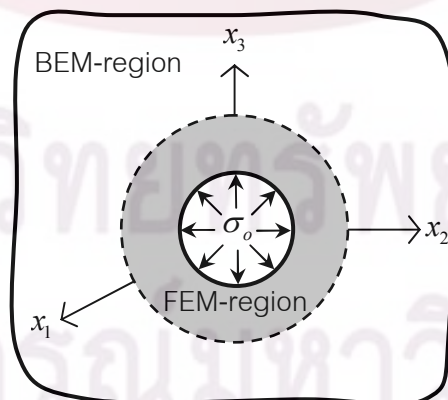


Figure 4.3 Decomposition of domain into BEM-region and FEM-region by a fictitious spherical surface of radius $5a$

In the analysis, three meshes are adopted as shown in Figure 4.4. While the meshes are shown only for the FEM-region, meshes for the BEM-region are identical to the interface meshes of the FEM-region. It is worth to point out that the level of refinement of all three meshes is significantly different. Specifically, Mesh 1 which is relatively coarse consists of 2 layers and each layer consists of 12 elements; Mesh 2 consists of 4 layers and each layer consists of 32 elements; and Mesh 3 consists of 8 layers and each layer consists of 144 elements.

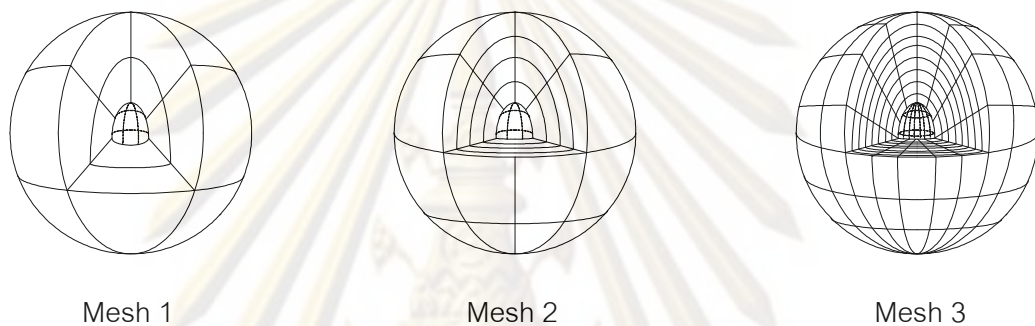


Figure 4.4 Schematic of three meshes used in the analysis

4.1.1 Isotropic linearly elastic material

For linear elasticity, this particular boundary value problem admits the closed form solution (e.g.). Since the problem is radial-symmetric, only radial displacement u_r and normal stress components $\{\sigma_{rr}, \sigma_{\theta\theta}, \sigma_{\phi\phi}\}$ are non-zero and they are given explicitly by (these components are with respect to a standard spherical coordinate system $\{r, \theta, \phi\}$ centered at the center of the void)

$$u_r(r) = \frac{(1+\nu)}{2E} \sigma_o \frac{a^3}{r^2} \quad (4.1)$$

$$\sigma_{rr} = -2\sigma_{\theta\theta} = -2\sigma_{\phi\phi} = -\sigma_o \left(\frac{a}{r}\right)^3 \quad (4.2)$$

This analytical solution is employed to validate the proposed formulation and the numerical implementation.

Numerical results for the radial displacement obtained from the three meshes are reported and compared with the exact solution in Figure 4.5. As evident from this set of results, solutions obtained from Mesh 2 and Mesh 3 are highly accurate while solutions obtained from Mesh 1 are reasonably accurate except in the region near the surface of the void. The discrepancy observed in Mesh 1 is due to that the level of refinement is not sufficient to accurately capture the geometry, loading condition, and the response in the local region near the surface of the void.

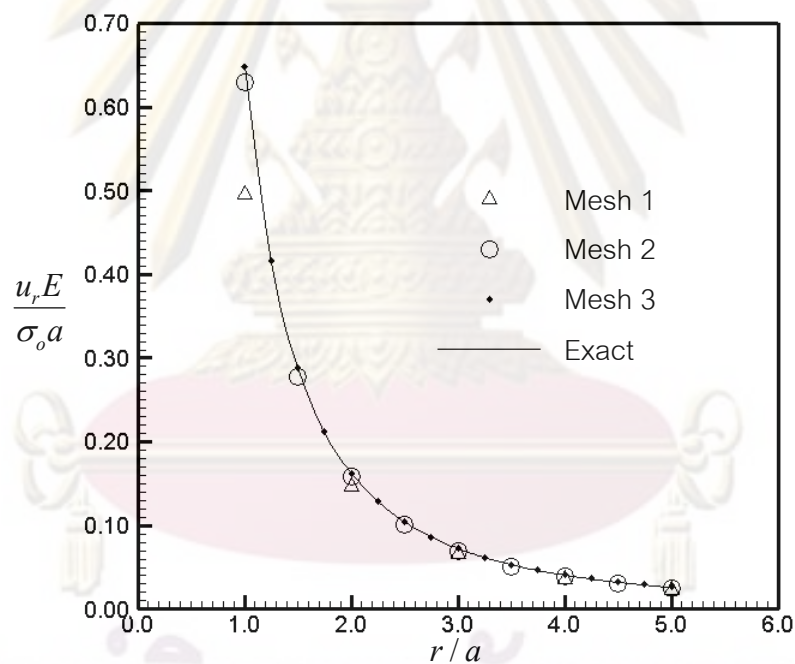


Figure 4.5 Normalized radial displacement versus the normalized radial coordinate for isotropic, linearly elastic material with $\nu = 0.3$

We further investigate the quality of numerical solutions for the stress. Since all non-zero stress components of the stress are related by (4.2), only results for the radial stress component are reported. Figure 4.6 shows results of the normalized radial stress obtained from all three meshes and the exact solution versus the

normalized radial coordinate. It is observed that Mesh 3 still yields results that are almost indistinguishable from the exact solution, while Mesh 1 and Mesh 2 give accurate results only for relatively large r and the level of accuracy decreases as the distance r approaches a . It is noted by passing that the degeneracy of the accuracy in computing stress is usual in a standard, displacement-based, finite element technique.

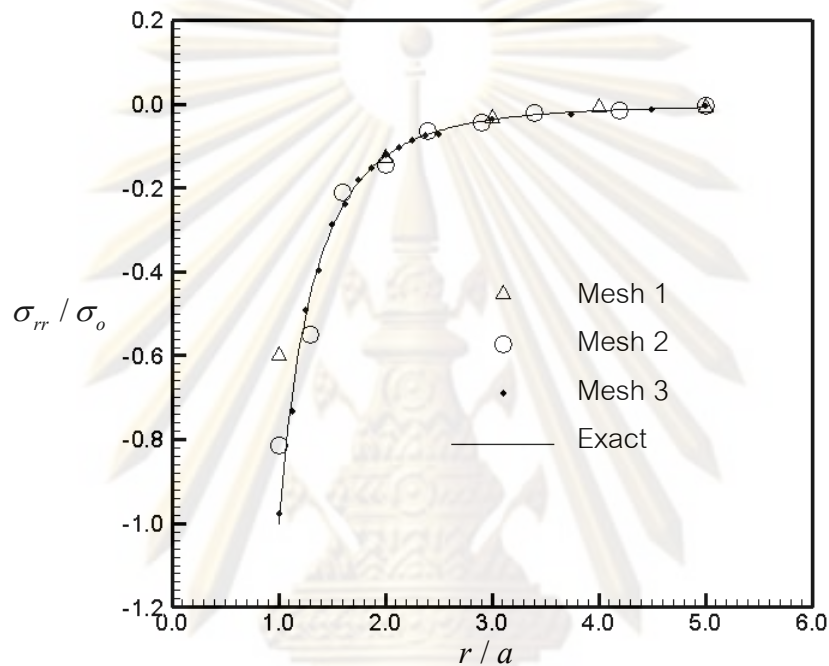


Figure 4.6 Normalized radial stress versus the normalized radial coordinate for isotropic, linearly elastic material with $\nu = 0.3$

To demonstrate the important role of the SGBEM in the treatment of an unbounded part of the domain instead of truncating the body to obtain a finite domain as practically employed in the FEM, we perform another FE analysis of the FEM-region without coupling with the BEM-region but instead imposing zero displacement condition. The radial displacement and radial stress obtained for this particular case using Mesh 3 are reported along with the exact solution and those obtained from the coupling technique in Figure 4.7 and Figure 4.8, respectively. As evident from results, numerical solutions obtained from the FEM with a domain truncation strategy are deviated from the exact solution when it moves close to the truncation surface while the proposed technique yields almost identical results to the exact solution.

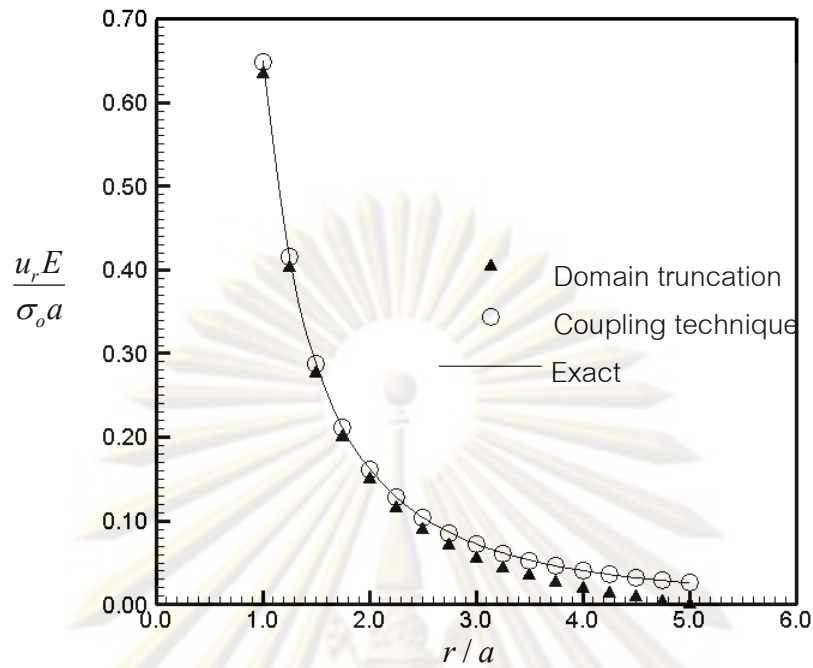


Figure 4.7 Normalized radial displacement versus the normalized radial coordinate for isotropic, linearly elastic material with $\nu = 0.3$. Results are obtained from Mesh 3 for both the coupling technique and the FE technique with domain truncation.

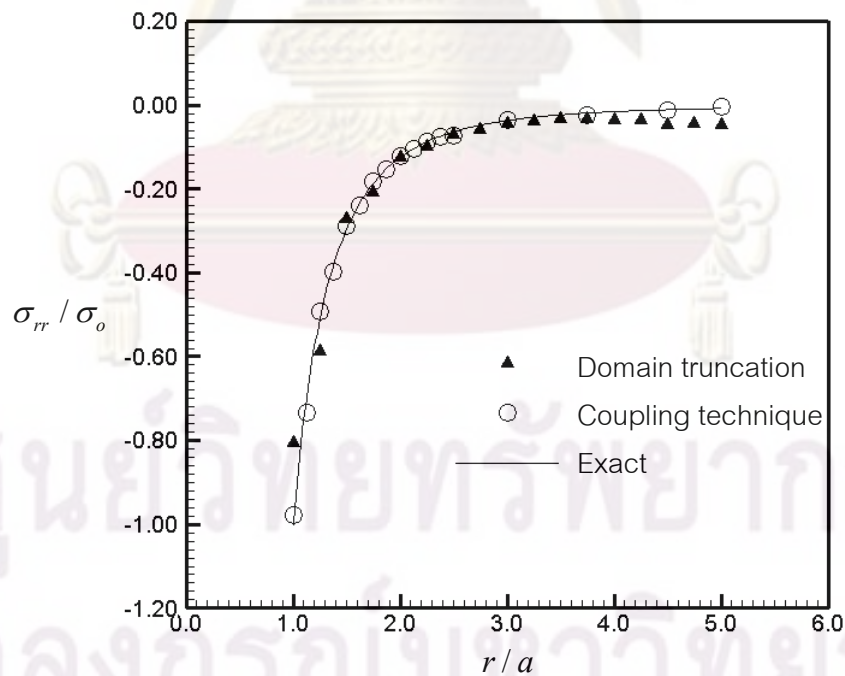


Figure 4.8 Normalized radial stress versus the normalized radial coordinate for isotropic, linearly elastic material with $\nu = 0.3$. Results are obtained from Mesh 3 for both the coupling technique and the FE technique with domain truncation.

4.1.2 Isotropic hardening material

For this particular case, we focus attention to the material with no hardening modulus (i.e. $E_2 = 0$) since the corresponding boundary value problem admits the close form solution. For a sufficiently high applied pressure σ_o , a layer close to the surface of void is inelastic and the size of such inelastic zone (measured by the radius r_o) becomes larger as σ_o increases. By incorporating J_2 flow theory of plasticity and symmetry along with equilibrium equation and strain-displacement relation, the radial displacement and the radial stress can readily be obtained as given below.

$$u_r(r) = \frac{1-2\nu}{E} \left\{ 2\sigma_y \ln\left(\frac{r}{a}\right) - \sigma_o \right\} r + \frac{1-\nu}{E} \sigma_y \frac{r_o^3}{r^2} \quad ; \quad r < r_o \quad (4.3)$$

$$\frac{\sigma_y}{3E} \left\{ (1+\nu) \frac{r_o^3}{r^3} \right\} r \quad ; \quad r > r_o$$

$$\sigma_{rr}(r) = 2\sigma_y \ln\left(\frac{r}{a}\right) - \sigma_o \quad ; \quad r < r_o \quad (4.4)$$

$$-\frac{2}{3} \sigma_y r_o^3 \left(\frac{1}{r^3}\right) \quad ; \quad r > r_o$$

where the Poisson ratio ν is taken to be 0.3 and r_o is the radius of an inelastic zone given by

$$r_o = ae^{\left(\frac{\sigma_o - 1}{2\sigma_y - 3}\right)} \quad (4.5)$$

In the analysis, we take the pressure $\sigma_o = 1.625\sigma_y$ to ensure that the body contains an inelastic zone; in fact, this selected applied pressure corresponds to $r_o = 1.615a > a$. Numerical results obtained from the coupling technique are reported along with the exact solution in Figure 4.9 for the normalized radial displacement and in Figure 4.10 for the normalized radial stress. It can be concluded from computed solutions that they converge to the exact solution as the mesh is refined.

In particular, results obtained from Mesh 3 are nearly indistinguishable from the benchmark solution. It is worth noting that results obtained from the same level of mesh refinement are less accurate than those for the linear elasticity case. This is due to complexity posed by the presence of an inelastic zone near the surface of the void and, to capture this phenomenon accurately, it therefore requires sufficiently fine meshes.

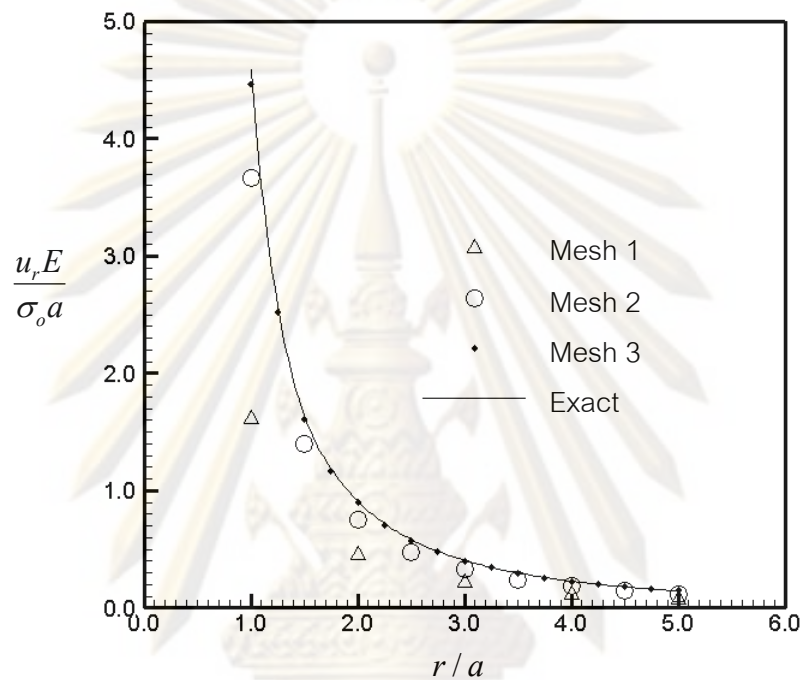


Figure 4.9 Normalized radial displacement versus the normalized radial coordinate for isotropic hardening material with $E_2 = 0$

4.2 Penny-shaped crack in an infinite media

Consider a penny-shaped crack of radius a which is embedded in a linearly elastic, infinite medium as shown schematically in Figure 4.11(a). The constituting material is assumed to be either an isotropic material with Poisson ratio $\nu = 0.3$ or zinc and graphite-reinforced composite. The last two materials are transversely isotropic with the axis of material symmetry oriented along the x_3 -axis and their elastic constants as shown in Table 4.1 can be found in the work of Kassir and Sih (1975) and Hyer (1998). The crack is assumed to be subjected to two types of traction boundary conditions: the uniform normal traction σ_0 (i.e. $t_1 = t_2 = 0$, $t_3 = \sigma_0$) as indicated in Figure

4.11(b) and the uniform shear traction τ_0 along the x_1 -axis (i.e. $t_1 = \tau_0$, $t_2 = t_3 = 0$) as shown in Figure 4.11(c).

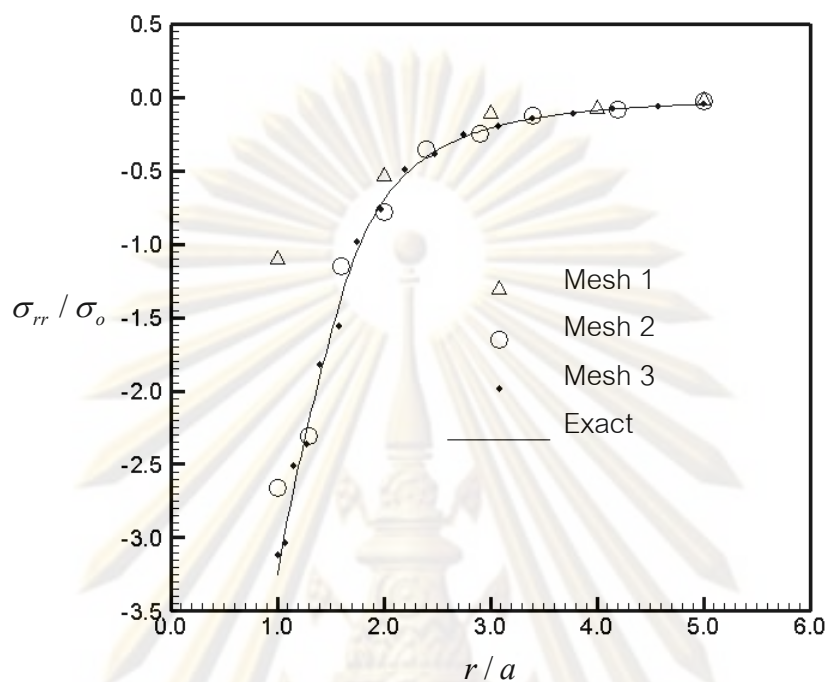


Figure 4.10 Normalized radial stress versus the normalized radial coordinate for isotropic hardening material with $E_2 = 0$

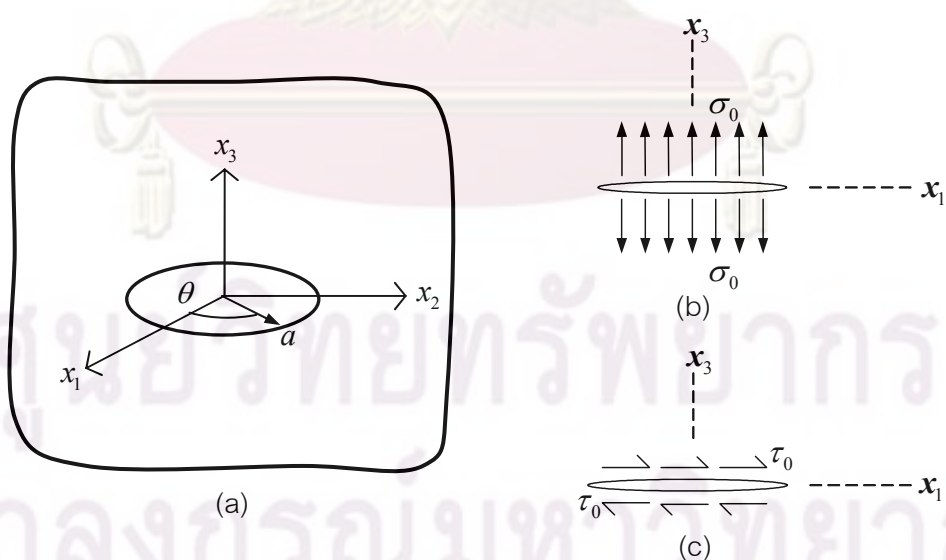


Figure 4.11 (a) Schematic of an infinite medium containing a penny-shaped crack, (b) crack under uniform normal traction σ_0 and (c) crack under uniform shear traction τ_0

Table 4.1 Elastic constants of zinc and graphite-reinforced composite (e.g. Kassir and Sih, 1975; Hyer, 1998). The axis of material symmetry is taken to direct along the x_3 -coordinate direction.

Elastic constants	$(\times 10^6)$ psi	
	Zinc	Graphite
E_{1111}	16.09	14.683
E_{1122}	3.35	6.986
E_{1133}	5.01	5.689
E_{3333}	6.10	144.762
E_{1313}	3.83	4.050

The first loading condition gives rise to an opening-mode problem with the mode-I stress intensity factor being constant along the crack front and independent of material properties while the second loading condition yields non-zero mode-II and mode-III stress intensity factors that vary as a function of position along the crack front. The analytical solutions of the two cases can be found in the work of Fabrikant (1989). As a means to verify the coupling formulation and implementation, we choose a cube of material of dimensions $2a \times 2a \times 2a$ centered at $(0, 0, 2a)$ as indicated in Figure 4.12 and define it as a FEM-region. In the analysis, we generate three meshes for both the crack surface and the FEM-region as depicted in Figure 4.13.

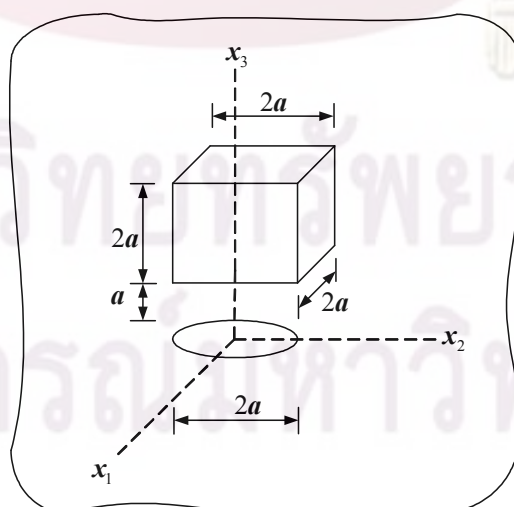


Figure 4.12 Schematic of a selected FEM-region and the remaining BEM-region

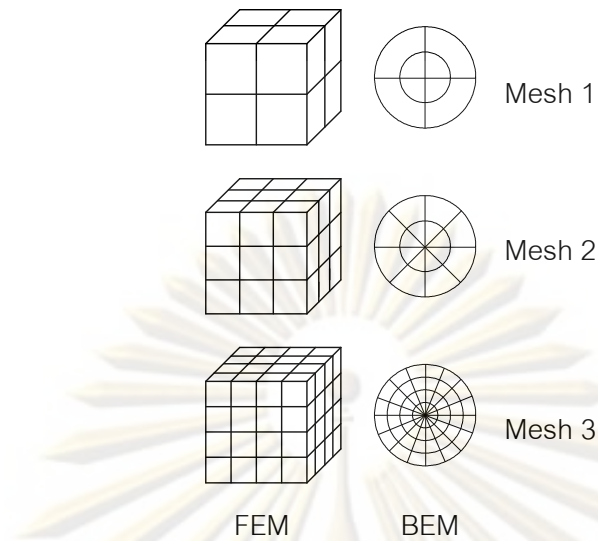


Figure 4.13 Schematic of three meshes used in the analysis

For the first loading condition, numerical solutions for the mode-I stress intensity factor normalized by the exact solution are reported in Table 4.2 for three materials and three meshes. Clearly from results obtained, the current technique yields highly accurate stress intensity factor with error less than 1.5%, 0.6% and 0.1% for Mesh 1, Mesh 2 and Mesh 3, respectively. This implies that the numerical solutions exhibit only weak dependence on the mesh refinement and a relatively coarse mesh can be used to generate results of sufficient accuracy.

Table 4.2 Normalized mode-I stress intensity factor for penny-shaped crack subjected to uniform normal traction

Mesh	Isotropic material $K_I / K_{I,ex}$		Transversely isotropic material $K_I / K_{I,ex}$			
			Zinc		Graphite	
	$\theta^\circ = 0$	$\theta^\circ = 90$	$\theta^\circ = 0$	$\theta^\circ = 90$	$\theta^\circ = 0$	$\theta^\circ = 90$
1	0.9919	0.9920	0.9890	0.9890	0.9841	0.9841
2	1.0008	1.0008	1.0001	1.0001	1.0053	1.0053
3	1.0002	1.0002	1.0004	1.0004	1.0006	1.0001

For the second loading condition, the normalized mode-II and mode-III stress intensity factors (K_2 and K_3) are reported in Figure 4.14, Figure 4.15 and Figure 4.16 for isotropic material, zinc and graphite-reinforced composite, respectively. Based on this set of results, it can be concluded that numerical solutions obtained from the three meshes are in excellent agreement with the exact solution; in particular, a coarse mesh also yields results of sufficient accuracy. This capability of the proposed technique is due to the use of special crack-tip elements to model the relative crack-faced displacement in the vicinity of the crack front. It is remarked that for this particular loading condition, the material anisotropy play an important role on the values of the mixed-mode stress intensity factors.

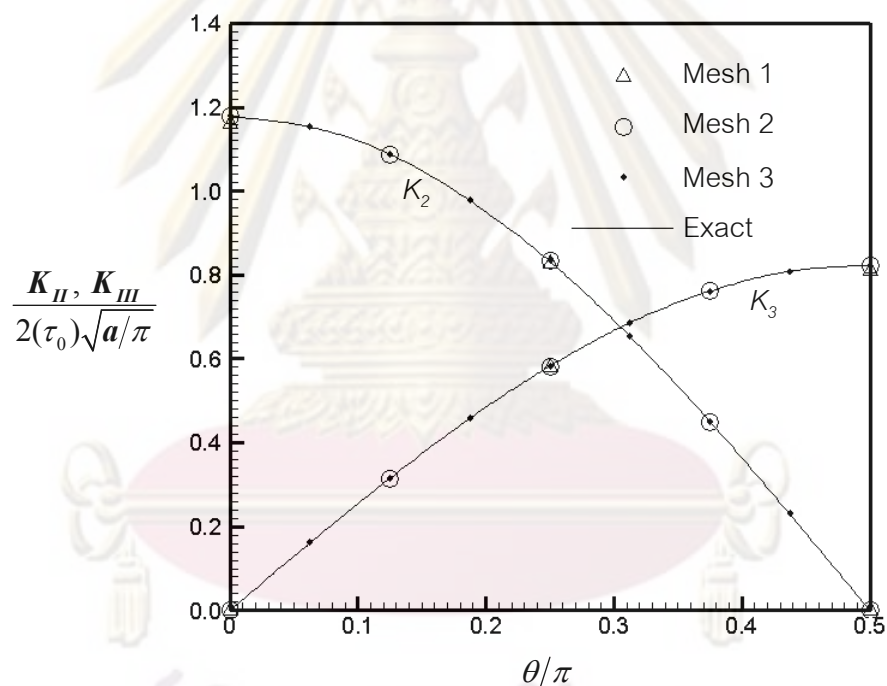


Figure 4.14 Normalized mode-II and mode-III stress intensity factor for penny-shaped crack subjected to shear traction. Results are reported for isotropic material with $\nu = 0.3$

4.3 Penny-shaped crack in an infinite media containing a spherical void

As a final example, we choose to test the current technique by solving a more complex boundary value problem in order to demonstrate its capability. Consider an infinite medium containing a spherical void of radius a and a penny-shaped crack of radius as shown schematically in Figure 4.17.

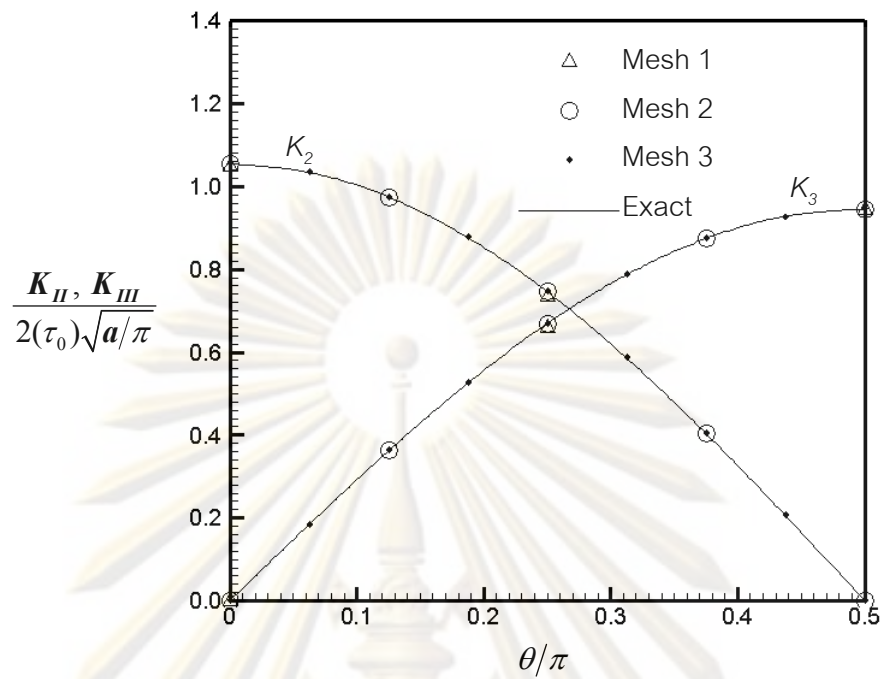


Figure 4.15 mode-II and mode-III stress intensity factor for penny-shaped crack subjected to shear traction. Results are reported for zinc.

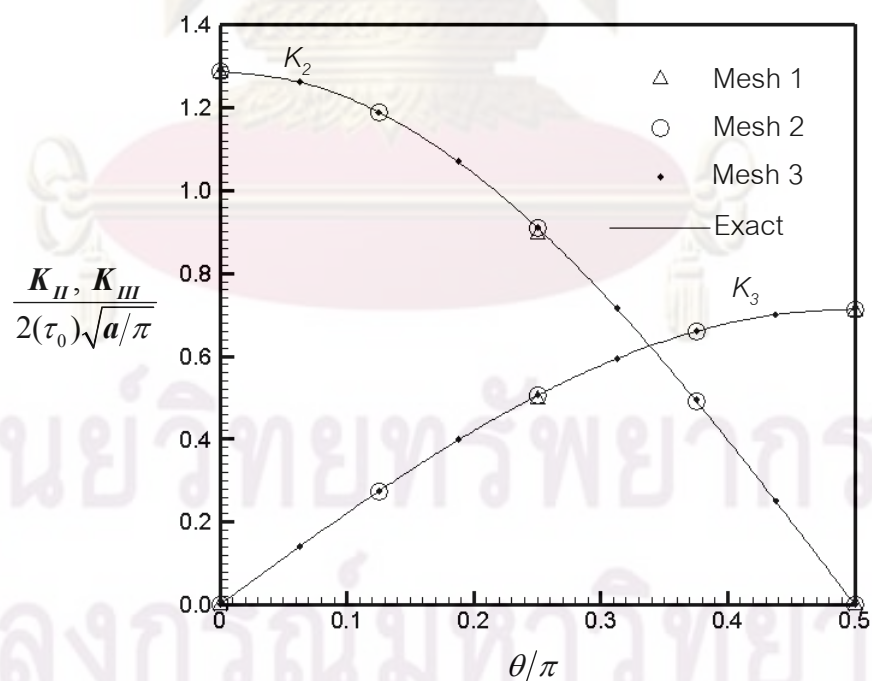


Figure 4.16 mode-II and mode-III stress intensity factor for penny-shaped crack subjected to shear traction. Results are reported for graphite reinforced-composite

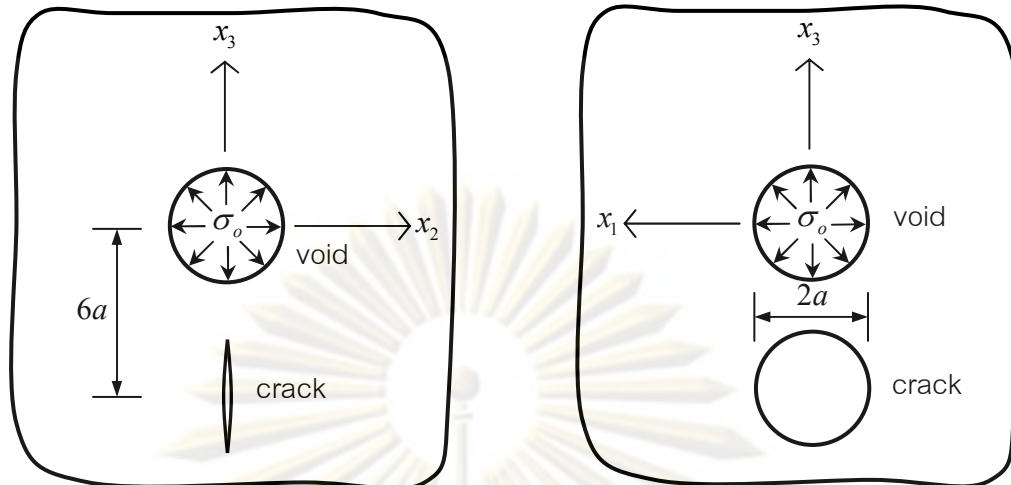


Figure 4.17 Schematic of a three-dimensional infinite medium containing a spherical void of radius a and a crack of radius a and subjected to uniform pressure at the surface of the void

The body is subjected to uniform pressure σ_0 on the surface of the void while the entire surface of the crack is traction free. In the analysis, two material models are investigated: one associated with an isotropic, linearly elastic material with Young's modulus E and Poisson ratio $\nu = 0.3$ and the other corresponding to an isotropic hardening material with the uniaxial stress-strain relation shown in Figure 4.2. The primary quantity of interest to be sought is the mode-I stress intensity factor along the crack front induced by the application of the pressure to the void. In addition, influence of an inelastic zone induced in the high load intensity region on such fracture data is also of interest.

In the modeling, we first decompose the body into the FEM-region and the BEM-region using a spherical surface of radius $4a$ centered at the same location as the void as shown schematically in Figure 4.18. Three meshes are adopted as shown in Figure 4.19. In particular, the FEM-region, the interface and the crack surface consists of $\{24, 12, 8\}$, $\{128, 32, 16\}$, and $\{1024, 128, 64\}$ elements for Mesh 1, Mesh 2 and Mesh 3, respectively. It is noted also that Mesh 1 is extremely coarse; for instance, only eight elements are utilized to discretize the entire crack surface and only four relatively large crack-tip element are used along the crack front.

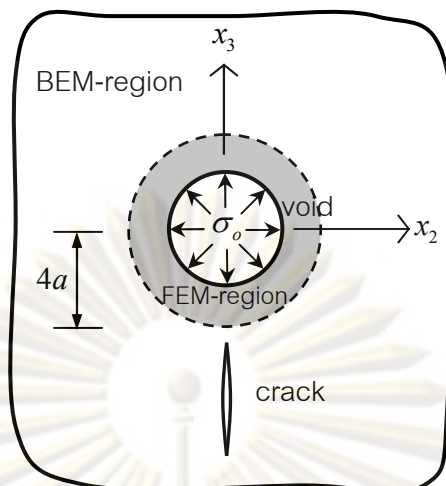


Figure 4.18 Decomposition of domain into BEM-region and FEM-region by a fictitious spherical surface of radius $4a$

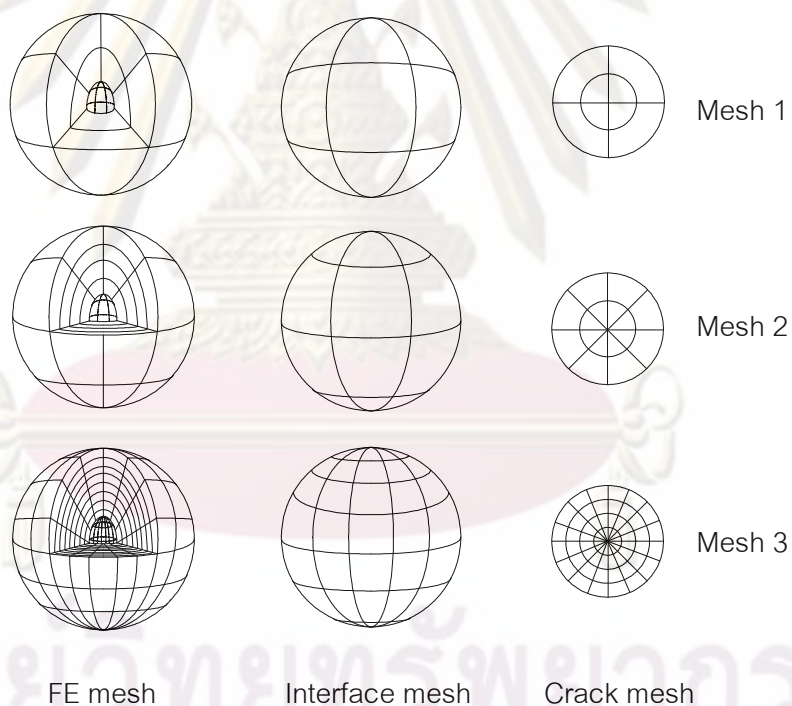


Figure 4.19 Schematic of three meshes used in the analysis

First, the analysis is carried out for the elastic material with Poisson ratio $\nu = 0.3$ and the computed mode I stress intensity factors are normalized and then reported as a function of angular position along the crack front for all three meshes in Figure 4.20. This set of results implies that the obtained numerical solutions exhibit good

convergence; in particular, results obtained from Mesh 2 and Mesh 3 are about the same quality while results obtained Mesh 1 still deviate from the converged solution. As is ensured by this convergence study, only Mesh 3 will be used to generate other sets of useful results.

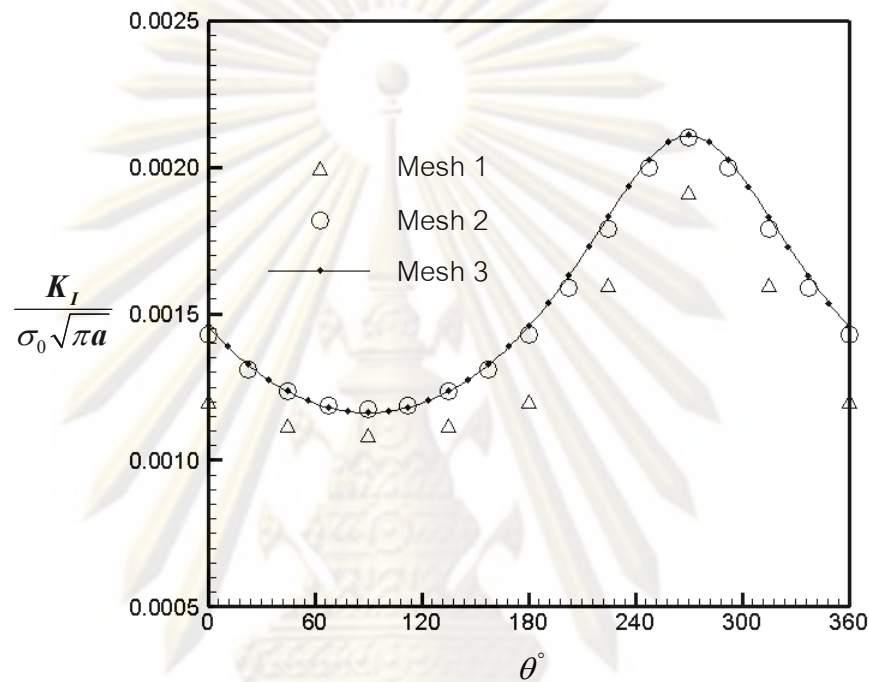


Figure 4.20 Normalized mode-I stress intensity factors for crack subjected to uniform pressure at the surface of void

Next, we consider a body made from an isotropic hardening material. In the analysis, we choose the modulus $E_1 = E$ and Poisson ratio $\nu = 0.3$ for linear regime and choose $E_2 = E/3$ and $E_2 = 0$ for hardening regime. With this set of material parameters, the linear behavior is identical to that considered in the problem of linear elasticity. To investigate the influence of the inelastic zone induced near the surface of the void on the stress intensity factor along the crack front, we carry out various experiments by varying the applied pressure σ_0 . The distribution of the stress intensity factor along the crack front (obtained from Mesh 3) is reported in Figure 4.21 for a hardening material with $E_1 = E$ and $E_2 = E/3$ under five levels of the applied pressure $\sigma_0 \in \{0.25\sigma_y, 1.00\sigma_y, 1.25\sigma_y, 1.50\sigma_y, 1.75\sigma_y\}$. The body is entirely elastic at

$\sigma_0 = 0.25\sigma_y$, slightly passes the initial yielding at $\sigma_0 = 1.00\sigma_y$, and possesses a larger inelastic zone as σ_0 increases further. It is obvious from Figure 4.21 that the presence of an elastic zone significantly alters the normalized value of the stress intensity factor from the linear elastic solution and such discrepancy becomes more obvious as the level of applied pressure increases. The localized inelastic zone acts as a stress riser; i.e., it produces stress field of higher intensity around the crack and this therefore yields the higher normalized stress intensity factor when compared with the linear elastic case. Figure 4.22 shows an additional plot between the maximum normalized stress intensity factors versus the normalized applied pressure for both an isotropic linearly elastic material and two isotropic hardening materials. Results for both types of materials are identical for a low level of the applied pressure (the entire body is still elastic) and, for a higher level of the applied pressure, the maximum stress intensity factor for the case of the hardening material is significant larger than that for the linear elastic material. In addition, such discrepancy tends to increase as the hardening modulus decreases.

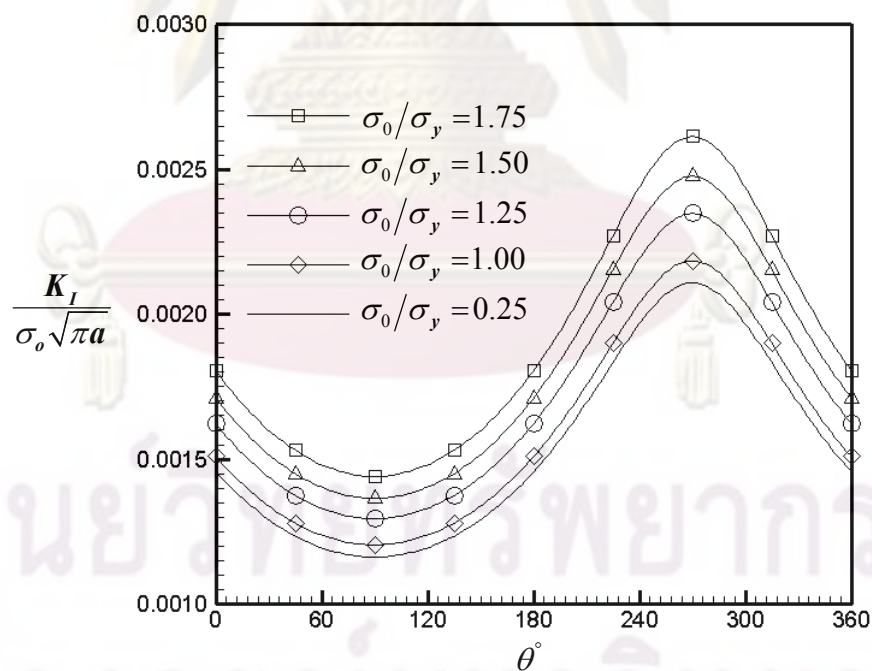


Figure 4.21 Normalized mode-I stress intensity factor for crack subjected to uniform pressure at the surface of void. Results are reported for isotropic hardening material ($E_1 = E, E_2 = E/3$) with different levels of applied pressure.

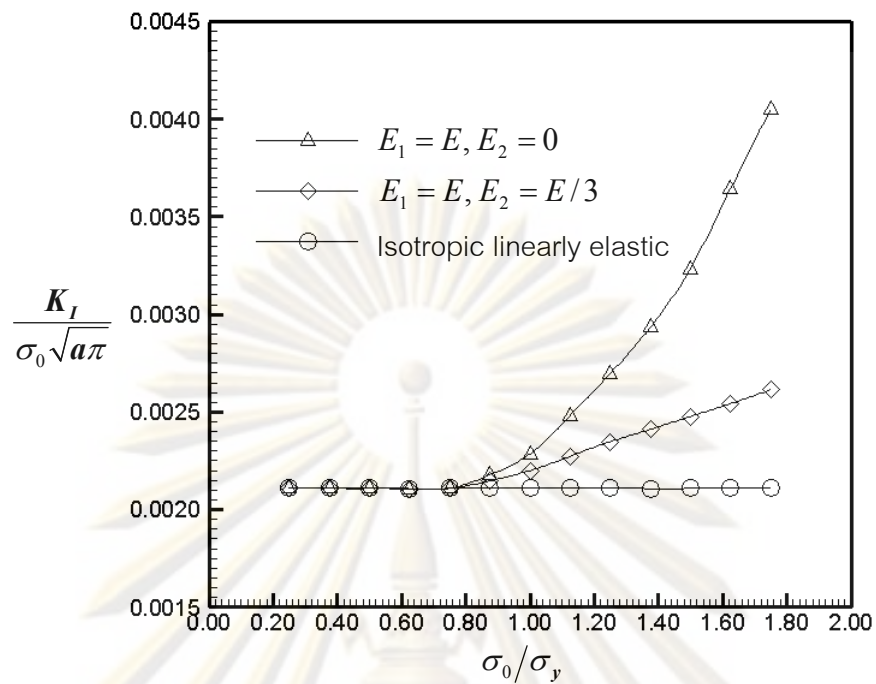


Figure 4.22 Maximum normalized mode-I stress intensity factor versus the level of applied pressure at the surface of void. Results are reported for an isotropic linearly elastic and two isotropic hardening materials.

ศูนย์วิทยทรัพยากร
จุฬาลงกรณ์มหาวิทยาลัย

CHAPTER 5

CONCLUSIONS AND REMARKS

A coupling between a standard finite element method (FEM) and a weakly singular, symmetric Galerkin boundary element method (SGBEM) has been successfully established for stress analysis of three-dimensional infinite media. The crucial feature of the current technique is to exploit the positive features of both the FEM and SGBEM to enhance the modeling capability. The vast and general features of the FEM has been employed to treat a complex, localized region that may contains inelastic zones or inhomogeneities while the SGBEM has been used to model the majority of the body that is unbounded and may contain the surface of discontinuity such as cracks.

The coupling formulation is based on the domain decomposition along with the proper enforcement of continuity of the displacement and traction on the interface of the two regions (one modeled by the SGBEM and the other treated by the FEM). For the FEM domain, the key formulation follows from the well-known principle of virtual work. For the SGBEM domain, the governing integral equation is formulated based on a pair of weakly singular, weak-form integral equations for the displacement and the traction. The final set of integral equations for the SGBEM domain is in a form well-suited for combining with that for the FEM domain to result in a symmetric weak formulation. In addition, all kernels involved in all integrals are only weakly singular of order $1/r$. This feature is crucial since it allows a space of continuous interpolation functions be employed everywhere in the discretization.

In the numerical implementation, various strategies have been employed to enhance both the accuracy and computational efficiency of the technique. For instance, the special crack-tip elements have been employed to discretize the local region along the crack front. The shape functions of these crack-tip elements have properly been enriched by a square root function such that the resulting interpolation

function can capture the relative crack-face displacement to sufficiently high order of accuracy. As a result, it allows relatively large crack-tip elements be used along the crack front while still yield very accurate stress intensity factors. Another attractive feature of the crack-tip element is its extra degrees of freedom on the edge along the crack front that are directly related to the gradient of the relative crack-face displacement. This renders all the stress intensity factors being extracted directly in terms of such extra degrees of freedom. Another important consideration is the use of an interpolation strategy to approximate values of kernels for generally anisotropic materials; this substantially reduces the computational cost associated with the direct evaluation of the line integral. Finally, special numerical quadratures have been adopted to accurately and efficiently evaluate the weakly singular and nearly singular double surface integrals.

To demonstrate and gain an insight into the coupling strategy, the formulation has been implemented first in terms of an in-house computer code for linear elasticity boundary value problems. Subsequently, the weakly singular SGBEM has successfully been coupled with a reliable commercial finite element package in order to exploit its vast capabilities to model a complex region such as inelastic zones and inhomogeneities. As indicated by results from extensive numerical experiments, the current technique yields highly accurate numerical solutions when compared with available benchmark solutions, and results exhibit good convergence and weak dependence on the level of mesh refinement.

As a final remark, while the developed technique is still restricted to an infinite domain and to matching or conforming interfaces, it offers insight into the SGBEM-FEM coupling strategy in terms of the formulation, the implementation procedure and its performance. This coupling strategy can directly be generalized to solve more practical boundary value problems involving a half-space, e.g. cracks and localized complex zone near the free surface. Another crucial extension is to enhance the feature of the current technique by using the weak enforcement of continuity across the interface. This will provide flexibility of the mesh generation.

REFERENCES

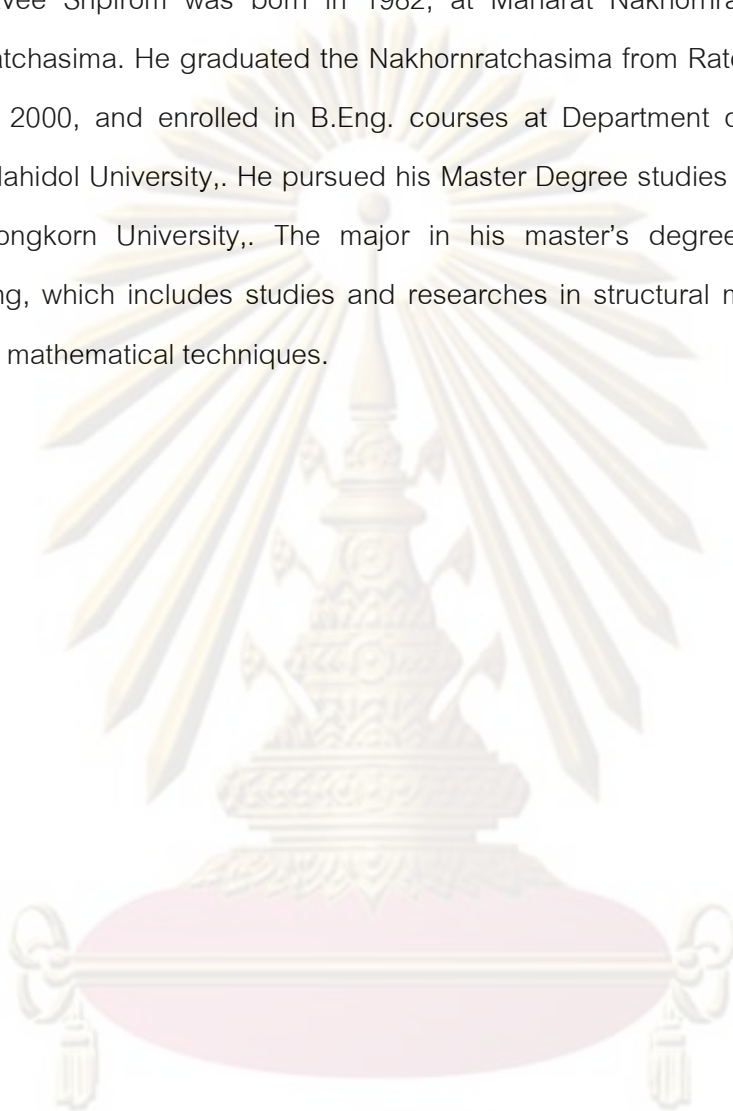
- Ayhan, A.O., A.C., Laflen, J., McClain, R.D. and Slavik, D. (2003). Fracture analysis of cracks in orthotropic materials using ANSYS. Reports No. GRC370. GEGlobal Research. General Electric Company.
- Bonnet, M. (1995). Regularized direct and indirect symmetric variational BIE formulations for three-dimensional elasticity. Engrg. Anal. Bound. Elem. Vol. 15: 93-102
- Bonnet, M., Maier, G. and Polizzotto, C. (1998). Symmetric Galerkin boundary element methods. Appl. Mech. Rev. 51: 669-703.
- Cruse, T.A. (1988). Boundary element analysis in computational fracture mechanics. Kluwer Academic Publishers. Dordrecht.
- Elleithy, W.M., Al-Gahtani, H.J. and El-Gebeily, M. (2001). Iterative coupling of BE and FE methods in electrostatics. Engrg. Anal. Bound. Elem. 25: 685-695.
- Elleithy, W.M and Tanaka, M. (2003). Interface relaxation algorithms for BEM-BEM coupling and FEM-BEM coupling. Comp. Methods Appl. Mech. Engrg Vol. 192: 2977-2992.
- Fabrikant, V.I. (1989). Application of potential theory in mechanics: a selection of new results Kluwer Academic Publishers Dordrecht.
- Fabrikant, V.I. (1991). Mixed boundary value problems of potential theory and their applications in engineering. Kluwer Academic Publishers Dordrecht.
- Frangi, A., Novati, G., Springhetti, R., and Rovizzi, M. (2002). 3D fracture analysis by symmetric Galerkin BEM. Comput. Mech. Vol. 28: 220-232.
- Frangi, A. and Novati, G. (2003). BEM-FEM coupling for 3D fracture mechanics application. Comput. Mech. Vol. 32: 415-422.
- Gray, L.J., Martha, L.F. and Ingrassia, A.R. (1990). Hypersingular integrals in boundary element fracture analysis. Int. J. Numer. Methods Engrg. 29: 1135-1158.
- Ganguly, S., Layton, J.B. and Balakrishna, C. (2000). Symmetric coupling of multi-zone curved Galerkin boundary elements with finite elements in elasticity. Int. J. Numer. Methods Engrg. 48: 633-654.

- Hayami, K. and Brebbia, C.A. (1988). Quadrature methods for singular and nearly singular integrals in 3-D boundary element method. Boundary Element X. Vol. 1. 237-264. Springer-Verlag: Berlin,
- Hyer, M.W. (1998). Stress analysis of Fiber-Reinforced Composite Material, McGraw-Hill, New York
- Hughes, T.J.R. (2000). The finite element method: linear static and dynamic finite element analysis. Dover Publications. New Jersey.
- Hass, M. and Kuhn, G. (2003). Mixed-dimensional, symmetric coupling of FEM and BEM. Engrg. Anal. Bound. Elem. Vol. 27: 575-582.
- Li, S., Mear, M.E. and Xiao, L. (1998). Symmetric weak-form integral equation method for three-dimensional fracture analysis. Comp. Methods Appl. Mech. Engrg. Vol. 151: 435-459.
- Martha, L.F., Wawrzynek, P.A. and Ingraffea, A.R. (1993). Arbitrary crack representation using solid modeling. Engrg. With Computers. Vol. 9: 63-82.
- Martin, P.A. and Rizzo, F.J. (1996). Hypersingular integrals: how smooth must the density. Int. J. Numer. Methods Engrg. 39: 687-704.
- Oden, J.T. and Carey, G.F. (1984). Finite elements: Special problems in solid mechanics. Vol. 5. Prentice-Hall: New Jersey.
- Rungamornrat, J. (2004). A computational procedure for analysis of fractures in three dimensional anisotropic media. Ph.D. Dissertation. The University of Texas at Austin. Texas.
- Rungamornrat, J. (2006). Analysis of 3D cracks in anisotropic multi-material domain with weakly singular SGBEM. Engrg. Anal. Bound. Elem. 30: 834-846.
- Rungamornrat, J and Mear, M.E. (2008). Weakly-singular, weak-form integral equations for cracks in three-dimensional anisotropic media. Int. J. Solids Struct. Vol. 45: 1283-1301.
- Rungamornrat, J and Mear, M.E. (2008). A weakly-singular SGBEM for analysis of cracks in 3D anisotropic media. Comp. Methods Appl. Mech. Engrg. Vol. 197: 4319-4332.

- Swenson, A.R. and Ingraffea, A.R. (1988). Modeling mixed-mode dynamic crack propagation using finite elements: theory and application. Comput. Mech. Vol. 3: 381-397.
- Schnack, E. and Turkey, K. (1997). Domain decomposition with BEM and FEM. Int. J. Numer. Methods Engng. 40: 2593-2610.
- Timoshenko, S. and Goodier, N. (1951). The theory of elasticity. 2nd edition. McGrawHill. New York.
- Xu, G. and Ortiz, M. (1993). A variational boundary integral method for the analysis of 3-D cracks of arbitrary geometry modeled as continuous distributions of dislocation loops. Int. J. Numer. Methods Engng. Vol. 36: 3675-3701.
- Xiao, L. (1998). Symmetric weak-form integral equation method for three-dimensional fracture analysis. Ph.D. Dissertation. University of Texas at Austin. Texas.
- Xu, G. (2000). A variational boundary integral method for the analysis of three-dimensional cracks of arbitrary in anisotropic elastic solids. J. Appl. Mech. 67: 403-408.
- Yu, G.Y. (2003). A symmetric boundary element method/finite element method coupling procedure for two-dimensional elastodynamic problems. J. Appl. Mech. 70: 451-454.
- Zienkiewicz, O.C. and Taylor, R.L. (2000). The finite element method: Solid mechanics. Vol 2: Butterworth-Heinemann. Oxford.

BIOGRAPHY

Mr. Sakravee Sripirom was born in 1982, at Maharat Nakhornratchasima Hospital, Nakhornratchasima. He graduated the Nakhornratchasima from Ratchasima Witthayalai School in 2000, and enrolled in B.Eng. courses at Department of Civil Engineering Faculty, Mahidol University,. He pursued his Master Degree studies in Civil Engineering at Chulalongkorn University,. The major in his master's degree is structural civil engineering, which includes studies and researches in structural mechanics and with advanced mathematical techniques.



ศูนย์วิทยทรัพยากร
จุฬาลงกรณ์มหาวิทยาลัย